Isotropic-nematic transition in shear flow: State selection, coexistence, phase transitions, and critical behavior

Peter D. Olmsted*
Exxon Research and Engineering Company, Route 22 East, Clinton Township, Annandale, New Jersey 08801

Paul M. Goldbart†
Department of Physics, University of Illinois at Urbana-Champaign, 1110 West Green Street, Urbana, Illinois 61801-3080 and Materials Research Laboratory, University of Illinois at Urbana-Champaign, 104 South Goodwin Avenue, Urbana, Illinois 61801

(Received 10 March 1992)

Macroscopic fluid motion can have dramatic consequences near the isotropic-nematic transition in thermotropic liquid-crystalline fluids. We explore some of these consequences using both deterministic and stochastic descriptions involving coupled hydrodynamic equations of motion for the nematic order parameter and fluid velocity fields. By analyzing the deterministic equations of motion we identify the locally stable states of homogeneous nematic order and strain rate, thus determining the homogeneous nonequilibrium steady states which the fluid may adopt. By examining inhomogeneous steady states we construct the analog of a first-order phase boundary, i.e., a line in the nonequilibrium phase diagram spanned by temperature and applied stress, at which nonequilibrium states may coexist, and which terminates in a nonequilibrium analog of a critical point. From an analysis of the nematic order-parameter discontinuity across the coexistence line, along with properties of the interface between homogeneous states, we extract the analog of classical equilibrium critical behavior near the nonequilibrium critical point. We develop a theory of fluctuations about biaxial nonequilibrium steady states by augmenting the deterministic description with noise terms, to simulate the effect of thermal fluctuations. We use this description to discuss the scattering of polarized light by order-parameter fluctuations near the nonequilibrium critical point and also in weak shear flow near the equilibrium phase transition. We find that fluids of nematogens near an appropriate temperature and strain rate exhibit the analog of critical opalescence, the intensity of which is sensitive to the polarizations of the incident and scattered light, and to the precise form of the critical mode.

PACS number(s): 64.70.Md, 05.70.Ln, 05.70.Fh, 05.70.Jk

I. INTRODUCTION AND OVERVIEW

Coherent macroscopic shear flow can dramatically influence the nature of phase transitions in a wide variety of fluids, from simple binary mixtures (and simple fluids) [1] to complex fluids such as nematic [2, 3] and smectic [4] liquid crystals, and other lamellar phases [5]. One can identify at least two distinct effects of shear flow on condensed matter, the relative importance of which depends crucially on the nature of the system at hand. In simple systems, such as binary mixtures of simple fluids, the primary effect of flow is to advect, and thereby destroy, long-lived fluctuations [1, 6]. Physical consequences include the raising of the transition temperature and the modification of critical behavior. In complex fluids such as fluids of thermotropic nematogenic (i.e., melts of rodlike molecules that exhibit an equilibrium nematic phase at sufficiently low temperatures) flow has the additional primary effect of inducing order and, moreover, for sufficiently strong flow this ordering effect can produce a nonequilibrium critical point [2, 3, 7].

The purpose of this paper is to present a detailed description of the influence of shear flow on the isotropic-nematic (I-N) transition exhibited by thermotropic fluids of nematogens [2, 3, 7, 8]. We have in mind an experimental situation in which a thermotropic fluid of nematogens is maintained at constant temperature T and in a state of steady planar shear flow by an externally applied shear stress, as depicted in Fig. 1. Alternatively, the fluid may be confined, e.g., between rotating coaxial cylinders in a Couette cell, or in Poiseuille flow in a capillary tube. (We have not yet addressed the many interesting issues concerning spatial and spatio-temporal instabilities [9] that such a driven system may undergo.)

Our specific aims are (i) to present a description of the time evolution of the coupled nematic order-parameter and fluid velocity fields; (ii) to identify the homogeneous nonequilibrium steady states which the fluid may adopt; (iii) to examine inhomogeneous steady states and use them to construct the analog of a first-order phase boundary, i.e., a line in the nonequilibrium phase diagram spanned by temperature and shear stress, at which nonequilibrium states may coexist; (iv) to describe the nonequilibrium analog of a critical point in which the coexistence line terminates; (v) to extract the analog of equilibrium critical properties (i.e., critical exponents) near the nonequilibrium critical point, from an analysis of the order-parameter discontinuity across the coexistence line and the properties of the interface between homogeneous states; and (vi) to develop a theory of fluctuations

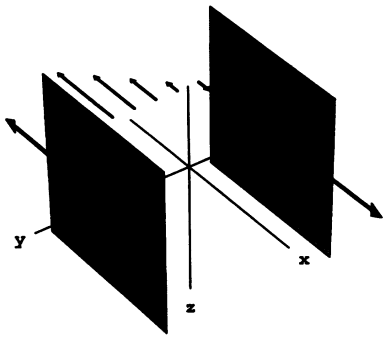

FIG. 1. Coordinate system for planar Couette flow, showing the boundary plates and fluid velocity field for a homogeneous state.

about biaxial nonequilibrium steady states, and to discuss the scattering of polarized light by nematic order-parameter fluctuations near the nonequilibrium critical point and also in weak shear flow near the equilibrium first-order I-N transition. As we shall see, fluids of nematogens undergoing shear flow near a certain critical strain rate and temperature exhibit the analog of critical opalescence, with an intensity which is sensitive to the polarizations of the incident and scattered light through the precise form of the critical mode.

Our treatment of fluctuations is at a level analogous to the Gaussian theory of equilibrium critical phenomena [10], and has similarities with related work on binary fluid [1], smectic [4], and other lamellar [5] systems. However, we find that the I-N system exhibits qualitatively new consequences of shear flow for fluctuations. In particular, in addition to aligning the nematogens and advecting large, long-lived fluctuations, flow makes possible divergent fluctuations at a nonequilibrium critical point. These fluctuations are analogous to critical fluctuations at the equilibrium liquid-gas critical point.

Fluctuations near the nonequilibrium critical point may be probed most readily through elastic light scattering, which we discuss in detail. At the nonequilibrium critical point of the flowing nematogens there is a single critical mode. This mode, however, differs from that at a conventional Ising-like critical point, being a superposition of orientation and amplitude modes of the order parameter. For the flowing nematogens the critical mode may be selectively probed by choosing suitable polarizations of incident and scattered light, whereas the analogous critical opalescence in the liquid-gas system is isotropic.

Throughout this work we shall mention certain concepts and phenomena familiar from the equilibrium liquid-gas system (which we henceforth refer to as LG; see, e.g., Ref. [11]). As we do this, it may be useful to bear in mind that such remarks apply equally to phase-separating binary fluids. In addition, it should be noted that we shall refer to homogeneous nonequilibrium steady states as phases.

In previous work [3,8,12] we have (i) presented the relevant coupled equations of motion for the order parameter and fluid velocity fields, valid for both uniaxial and biaxial molecular alignment of small magnitude; (ii) constructed a nonequilibrium phase diagram from the homogeneous solutions to these equations of motion; (iii) outlined a scheme for locating coexistence between nonequilibrium states; (iv) sketched a framework for analyzing nonequilibrium fluctuations and light-scattering; and (v) discussed analogies with equilibrium systems such as the LG.

References [3,8,12] were, however, all rather brief. We will, therefore, in the course of this presentation, find ourselves giving a detailed recapitulation of their contents. As we do this, we would like to stress the following two points which we have not previously emphasized. First, the criterion for determining coexistence of states within the two-state region is that the relevant states have a common momentum flux density (which is closely related to the *boundary stress*), as discussed in Sec. VI A. To the best of our knowledge, this criterion has not been explicitly addressed in the context of complex fluids, and phase diagrams for flowing systems have generally been constructed in terms of an imposed strain rate rather than applied shear stress [2, 3, 7, 13]. Indeed, it should be noted that while the stationary states themselves do not depend on the choice of control parameter (stress or strain rate) their stability is sensitive to this choice and, consequently, so is the precise location of the nonequilibrium critical point. Second, the quantity which vanishes as the critical point is approached along the coexistence line, i.e., the proper order parameter for the continuous transition, is constructed by an appropriate projection of the nematic order-parameter discontinuity on to a certain critical mode. The necessity for such a projection occurs because the principal axes of the nematic order-parameter discontinuity rotate, as the critical point is departed from along the coexistence line.

This paper is organized as follows. In Sec. II we give a brief discussion of the effects of shear flow on various mesophases of condensed matter. In Sec. III we summarize some important facts about the equilibrium I-N transition. In Sec. IV we present the equations of motion used to obtain our results. In Sec. V we review the homogeneous nonequilibrium steady states, presenting detailed expressions for the alignment in weak flow near the I-N transition. In Sec. VI we consider inhomogeneous nonequilibrium steady states and describe the interface construction used to analyze selection between, and coexistence of, such states, and present the resulting nonequilibrium phase diagram. From the interface construction we extract information about the critical behavior of the system which — not surprisingly, given our framework — turns out to correspond to classical equilibrium critical behavior. In Sec. VII we describe the dynamics of linear fluctuations about nonequilibrium steady states under shear flow, and in Sec. VIII we conclude this paper with a summary of our results and suggestions for future directions.

II. SIMPLE AND COMPLEX FLUIDS IN SHEAR FLOW

The paramount motivation for the study of fluids of mesogens (i.e., molecules forming phases intermediate be-

tween liquid and crystal), such as nematogens, in shear flow stems from the observation that such flow can influence the state of order at the molecular level. This fact suggests the possibility of flow-controlled transitions between states which differ in the degree, and perhaps nature, of their molecular alignment. Important additional motivation stems from the fact that shear flow introduces a new macroscopic time scale

$$\tau_D \equiv D^{-1}, \tag{2.1}$$

through the strain rate D. Equilibrium fluctuations with an intrinsic lifetime shorter than τ_D should barely be affected by the shear flow, while those with longer lifetimes should be strongly influenced (i.e., severely distorted by advection). Thus, one anticipates that the broad impact of shear flow is to suppress fluctuations; that this is indeed the case has been shown both theoretically [1] and experimentally [6] for the case of the near-critical binary fluid. However, for more complex fluids the manner and ramifications of the suppression of fluctuations depend on the precise nature of the ordering and fluctuations encountered in the equilibrium state.

A. Critical simple fluids under shear flow

The impact of shear flow on the binary fluid near its critical point was first investigated by Onuki and Kawasaki [1], whom we henceforth refer to as OK. Now, an equilibrium critical point is characterized, according to the scaling hypothesis [10, 14], by a diverging correlation length, which implies that fluctuations at the critical point occur on all length scales from microscopic to macroscopic. Furthermore, associated with a fluctuation at a particular wave number k is a characteristic time scale τ_k over which this fluctuation relaxes in equilibrium. This time scale should be compared with τ_D, which is, roughly speaking, a measure of how long it takes for a fluctuation to experience advection. If $\tau_D < \tau_k$, the fluctuation would be destroyed by advection more rapidly than it would relax in equilibrium. As longer wavelength fluctuations have longer characteristic time scales τ_k, the afflicted fluctuations are the longer wavelength ones, i.e., precisely those which are characteristic of a system near equilibrium criticality. Hence, fewer of the long-wavelength fluctuations contribute to the critical behavior, as the strain rate is increased, and one might expect to find classical rather than anomalous critical behavior [10]. In addition, shear flow frustrates the microscopic processes (i.e., van der Waals attraction) which induce the equilibrium LG critical point, leading to the suspicion that the critical temperature should be *reduced* in the presence of shear flow. These consequences of shear flow were predicted theoretically by OK using a renormalization-group (RG) strategy applied to a Fokker-Planck description of the coarse-grained dynamics, and verified experimentally, along with other predictions, by Beysens and co-workers [6].

B. The driven diffusive lattice gas

Related to the LG in shear flow is the driven diffusive lattice gas (DDLG) [15–17]. This model was proposed by Katz, Lebowitz, and Spohn [15] as a simple example of a nonequilibrium system whose behavior under an external driving field might provide insight into the general subject of nonequilibrium phase transitions. The model consists of a gas of particles, conserved in number, which are free to hop on a lattice. An effective external driving field is simulated by imposing anisotropic jump rates, so that jumps in a preferred direction are more probable than others. In addition, periodic boundary conditions are imposed, in order to accommodate flowing steady states. In the absence of the driving field the phase diagram is spanned by temperature and average particle density. At half-filling, the system segregates into high- and low-density regions at a critical point in the Ising universality class. The properties of this continuous transition, in the presence of a driving field, have been studied via numerical simulations [15], mean-field approximations [16], and field-theoretic techniques [17]. It has been determined that the transition remains continuous in the presence of the driving field, and that the critical temperature increases with increasing field, but that the universality class, and hence the critical behavior, differs from that of the equilibrium critical point. As with the LG [1], the driving field causes the correlations to become highly anisotropic, and classical critical behavior is found.

C. The isotropic-lamellar transition under shear flow

The isotropic-lamellar (I-L) transition occurs, e.g., in microemulsions and diblock copolymers [18, 19], and is a transition between an isotropic state and a one-dimensionally ordered state, thus having a higher degree of molecular organization than the LG. Such order is characterized by a wave vector of magnitude k_0 but arbitrary direction (neglecting boundary forces). The mean-field equilibrium transition, as dictated by symmetry considerations, can be of either second order or weakly first order. However, Brazovskiĭ [20] has predicted that strong fluctuations associated with the degeneracy in the direction of the ordering wave vector $\mathbf{k}_0$ should induce a first-order transition.

The I-L transition in shear flow has been studied theoretically by Cates and Milner and by Marques and Cates [5]. Having a higher degree of molecular organization than the LG, the I-L transition exhibits certain qualitative features also exhibited by the I-N transition under shear flow.

Inasmuch as fluctuations are suppressed, the effect of shear flow on the I-L and LG transitions is similar, but there are significant differences. Near both transitions, shear flow destroys those fluctuations with sufficiently long lifetimes. However, a special role is played in the I-L case by the lamellar nature of the ordered phase [5]: fluctuations which form with layers normal to the flow direction are quickly eradicated in flow, while fluctuations with layers parallel to the flow are more likely to survive. Hence, shear flow not only suppresses lamellar droplets *larger* than a given size, as with the LG, but also regulates the *class* of fluctuations which occur, and constrains the set of candidate low-temperature lamellar

phases. In contrast with the LG, the I-L transition temperature *increases* in the presence of shear flow, because certain fluctuations which frustrate equilibrium ordering are suppressed by the flow. The nature of the I-L transition in flow was predicted by Cates and Milner and by Marques and Cates, to cross over to mean-field–type at sufficiently high strain rates. Whereas equilibrium fluctuations in the layer orientation (i.e., Brazovskiĭ fluctuations [20]) induce a first-order transition, shear flow is predicted to restore a *continuous* mean-field transition, at least in the limit of infinite strain rate [5].

D. The nematic–to–smectic-A transition under shear flow

The nematic–to–smectic-A (N–Sm-A) transition under shear flow has been studied experimentally by Safinya, Sirota, and Plano [21], and theoretically by Bruinsma and Safinya [4]. The transition between nematic and smectic states is similar to the I-L transition, in that a one-dimensional density wave develops. This density wave may be crudely envisaged as comprising stacked layers of nematically aligned rodlike molecules. The effects of flow are similar to those on the I-L transition: advection suppresses long-wavelength fluctuations, and the layering direction is prescribed by the flow. Hence, the transition temperature should increase in flow and the behavior should be mean-field-like.

However, the N–Sm-A transition in shear flow has an additional complication due to the nematic order present in both N and Sm-A phases. Flow prescribes a direction for nematic ordering [22, 23], somewhat reminiscent of the alignment by a magnetic field of a ferromagnet below its Curie temperature. However, a nematic state in shear flow cannot undergo a transition to the smectic state in the same way that it does in equilibrium, with the smectic layer normal parallel to the orientation specified by the nematic alignment. The reason for this is that shear flow orients the mesogen molecules roughly parallel to the flow, whereas (as we have seen in the discussion of the I-L transition [5]) layers with normals parallel to the flow will be destroyed by advection: stable smectic layering can only occur in layers which do not cut across streamlines. Thus, there will be a crossover in the preferred rod orientation, e.g., as the temperature is reduced at fixed strain rate, from alignment roughly parallel to the flow in the nematic state, to alignment normal to the shear plane in the smectic state [4, 24]. Consequently, the phase diagram acquires much structure as shear stress is applied to the fluid [21]. Interesting additional predictions concerning the renormalization of the anisotropic viscosities (i.e., Leslie coefficients) [4, 24] have been made for the N–Sm-A fluid under shear flow.

E. The isotropic-nematic transition under shear flow

The isotropic-nematic (I-N) transition in shear flow has been studied by several researchers, beginning with Hess [2] and followed by Olmsted and Goldbart [3] and See, Doi, and Larson [7]. In addition, Thirumalai [25], Lee [26], and Wang and Gelbart [13] have studied the related problem of phase transitions in systems of rodlike molecules in uniaxial elongational flow. As noted first by Hess, the propensity of nematogens to align in shear flow causes the transition under flow to occur at a temperature higher than the equilibrium transition temperature. At sufficiently high strain rates a transition no longer occurs, and the state of the system evolves smoothly as the temperature is lowered.

The equilibrium transition, which is first order and occurs at a temperature $T_{I\text{-}N}$, is a symmetry-breaking transition from an isotropic state to a uniaxial nematic state [27], with Goldstone modes of director fluctuation accompanying the spontaneously broken symmetry [28]. Shear flow has two significant effects on the state of molecular alignment. First, it induces alignment in the nematogens and selects a particular orientation for this ordering. This should be contrasted with N–Sm-A and I-L transitions, for which flow directly affects the layering orientation but not, primarily, the magnitude of the molecular order. Second, planar shear flow has a biaxial symmetry, and hence both the high- and low-temperature states of nematogens in shear flow are, to some extent, biaxial, which renders the transition in flow a non-symmetry-breaking transition, reminiscent of the LG transition. In contrast, the symmetry-breaking nature of the I-L, N–Sm-A, and LG transitions are unaffected by the flow, at least with regard to static correlations. By analogy with other non-symmetry-breaking phase transitions, such as the LG transition, it is reasonable to anticipate that, as the applied shear stress is increased, a nonequilibrium analog of the discontinuous equilibrium I-N transition should terminate in a critical point (although, in principle, multicritical phenomena are possible). Furthermore, because flow suppresses the fluctuations which frustrate ordering of the system, the transition temperature should increase with increasing strain rate, as with the I-L and N–Sm-A transitions.

There are several important distinctions between the systems we have briefly examined, and it is worthwhile to review them. The LG has no long-range internal structure, and the advective action of flow on the fluctuations induces classical critical behavior. The N–Sm-A and I-L transitions are both transitions to states with long-range density structure, namely a one-dimensional density wave. For these, the effects of shear flow are twofold: (i) long-lived fluctuations are advected by flow and (ii) the orientation of the density wave vector is constrained to lie normal to the flow direction, resulting in an increase in the transition temperature. The symmetry-breaking nature of these transitions (i.e., from translational invariance to one-dimensional density wave) is preserved under shear flow. The nematic system also has long-range internal structure, but which couples *directly* to the flow gradient. Flow therefore affects both the magnitude and the orientation of the molecular ordering, as well as altering the symmetry-breaking nature of the transition. As we shall see, its effect is to raise the transition temperature, and to introduce a critical point into the nonequilibrium phase diagram.

III. EQUILIBRIUM NEMATIC FLUIDS

A. Nematic order parameter

To describe the local state of molecular alignment in a fluid of N nematogens we adopt the conventional nematic order parameter $Q_{\alpha\beta}(\mathbf{r},t)$ [29], defined by

$$\rho(\mathbf{r},t)\,Q_{\alpha\beta}(\mathbf{r},t)$$

$$=\sum_{a=1}^{N}\left\langle\left[\nu_\alpha^{(a)}(t)\nu_\beta^{(a)}(t)-\tfrac{1}{3}\delta_{\alpha\beta}\right]\delta(\mathbf{r}-\mathbf{r}^{(a)}(t))\right\rangle, \quad (3.1)$$

where $\mathbf{r}^{(a)}$ is the position of the ath rodlike molecule, $\boldsymbol{\nu}^{(a)}$ is the unit vector representing the orientation of the ath molecule, having Cartesian components $\nu_\alpha^{(a)}$ (with $\alpha=1,2,3$), and the angle brackets denote an appropriate ensemble average. We shall assume that the molecule (number) density, $\rho(\mathbf{r},t)\equiv\sum_{a=1}^{N}\langle\delta(\mathbf{r}-\mathbf{r}^{(a)}(t))\rangle$, is spatially uniform (i.e., homogeneous) and temporally constant. The subtraction of (one-third of) the identity in Eq. (3.1) ensures that the order parameter $Q_{\alpha\beta}$ vanishes for an isotropic state. The order parameter $Q_{\alpha\beta}(\mathbf{r},t)$ is thus a traceless and symmetric second-rank tensor field, having five kinematically independent internal degrees of freedom.

While states with isotropic or uniaxial distributions of molecular orientation are the most common equilibrium states for nematogens, the molecular orientation distribution function may have biaxial symmetry, either (i) spontaneously (which is rare) or (ii) due to a biaxial external field (such as shear flow), or, e.g., (iii) due to a magnetic field (when the magnetic susceptibility is negative). For a biaxial state, the order parameter takes the form

$$Q_{\alpha\beta}=\tfrac{3}{2}S_1\,(n_\alpha n_\beta-\tfrac{1}{3}\delta_{\alpha\beta})+\tfrac{1}{2}S_2\,(m_\alpha m_\beta-l_\alpha l_\beta), \quad (3.2)$$

where the orthogonal directors $\hat{\mathbf{n}}$, $\hat{\mathbf{m}}$, and $\hat{\boldsymbol{l}}$ are the principal axes of $Q_{\alpha\beta}$. The director $\hat{\mathbf{n}}$ indicates the primary direction of alignment; the subdirector $\hat{\mathbf{m}}$ indicates the secondary direction of alignment; and $\hat{\boldsymbol{l}}=\hat{\mathbf{n}}\times\hat{\mathbf{m}}$. The biaxial state is thus specified by five parameters: the uniaxial scalar amplitude S_1, the biaxial scalar amplitude S_2, two angles to specify the orientation of the director $\hat{\mathbf{n}}$, and a third angle to specify the rotation angle of $\hat{\mathbf{m}}$ about $\hat{\mathbf{n}}$. The uniaxial state, in which $S_2=0$, is specified by only three parameters: the magnitude S_1, and two angles to orient the director. S_1 and S_2 may also be interpreted in terms of moments of the molecular orientation distribution function $\psi\{\boldsymbol{\nu}\}$,

$$S_1=\langle\cos^2\theta-\tfrac{1}{3}\rangle=\langle\nu_z^2-\tfrac{1}{3}\rangle, \quad (3.3a)$$

$$S_2=\langle\sin^2\theta\cos 2\phi\rangle=\langle\nu_x^2-\nu_y^2\rangle, \quad (3.3b)$$

where θ and ϕ are the conventional spherical polar coordinates, the z axis is taken to be parallel to $\hat{\mathbf{n}}$, and $\langle\,\rangle$ here denotes an average over $\psi\{\boldsymbol{\nu}\}$.

B. Landau–de Gennes theory of the isotropic-nematic transition

Typically, equilibrium I-N transitions are found experimentally to be rather weak first-order transitions (commonly $S_1\sim 0.3$ [30]), so that a satisfactory qualitative description of them may be obtained by asserting that homogeneous equilibrium states (i.e., phases) minimize the Landau–de Gennes free-energy density [11, 31],

$$f_{\rm L}=\tfrac{1}{2}A(T)\,Q_{\alpha\beta}Q_{\beta\alpha}+\tfrac{1}{3}B\,Q_{\alpha\beta}Q_{\beta\gamma}Q_{\gamma\alpha}+\tfrac{1}{4}C\big(Q_{\alpha\beta}Q_{\beta\alpha}\big)^2. \quad (3.4)$$

(Implicit throughout this paper will be a summation from 1 to 3 over repeated greek subscripts representing Cartesian components.) The cubic term, allowed because $Q_{\alpha\beta}\to -Q_{\alpha\beta}$ is not a symmetry, ensures that the mean-field transition can be first-order [11]; a negative value for B gives the conventional uniaxial nematic state. The important temperature dependence is taken to reside in $A(T)\equiv a(T-T^-)$, while the variation of B and C with temperature T is assumed to be weak and will be neglected. The I-N transition occurs with a discontinuity $\Delta S_1=-2B/9C$ at a transition temperature $T_{I\text{-}N}$, given by $A(T_{I\text{-}N})=B^2/27C$ [30].

In addition to the Landau–de Gennes homogeneous free-energy density, we must also account for the free energy cost of spatial distortions [32]. For temperatures near $T_{I\text{-}N}$, where variations in amplitude occur relatively easily, the distortion (or Frank) free energy may be taken to be

$$f_F=\tfrac{1}{2}L_1\,(\partial_\alpha Q_{\beta\gamma})^2+\tfrac{1}{2}L_2\,(\partial_\alpha Q_{\alpha\beta})^2, \quad (3.5)$$

where L_1 and L_2 are elastic moduli. This is not the most general expression: we have ignored surface terms, terms of the same order in gradients but higher order in $Q_{\alpha\beta}$, and higher-order gradient terms. However, for bulk properties of systems near $T_{I\text{-}N}$, for which $Q_{\alpha\beta}$ is small, this form is adequate [29].

It is interesting to note that translational and rotational degrees of freedom are uncoupled when the modulus L_2 vanishes. In this case, the free energy is invariant under independent global rotations of the molecular center-of-mass locations and the molecular orientations, i.e., the symmetry group is then $\mathrm{O}(3)\otimes\mathrm{O}(3)$, rather than its diagonal subgroup $\mathrm{O}(3)$. Thus, with the approximation $L_2=0$ we expect certain properties associated with spatial gradients to be isotropic, so that calculations are extensively simplified, while — it is hoped — retaining much of the physics. We will employ this approximation, the so-called "one-constant approximation," in our analysis of steady-state correlations in shear flow (Sec. VII) [33]. (See Ref. [34] for one example of a situation in which adopting the one-constant approximation would be too drastic a simplification.)

Using the Landau–de Gennes and distortion contributions to the free-energy density, one may calculate the equilibrium correlations between certain thermally fluctuating quantities. For simplicity, we temporarily consider the one-constant approximation, $L_2=0$. At temperatures slightly higher than $T_{I\text{-}N}$ the system is isotropic

but, because of the weakness of the first-order transition, there are small, although significant, nematic fluctuations. As the fluctuations in the order parameter are small in this regime, it is adequate to truncate the Landau–de Gennes free energy after the quadratic term. The equilibrium fluctuations in the Fourier modes of the order parameter $Q_{\alpha\beta}(\mathbf{k})$ are then given by the equipartition theorem, i.e.,

$$\langle Q_{\alpha\beta}(\mathbf{k})Q_{\lambda\rho}(-\mathbf{k})\rangle = \frac{k_BT/2}{a(T-T^-)+L_1k^2}(\delta_{\alpha\lambda}\delta_{\beta\rho}+\delta_{\alpha\rho}\delta_{\beta\lambda}-\tfrac{2}{3}\delta_{\alpha\beta}\delta_{\lambda\rho}). \tag{3.6}$$

Here $\langle\mathcal{O}\rangle \equiv Z^{-1}\int\mathcal{D}Q\,\mathcal{O}\exp(-F/k_BT)$, where $\mathcal{D}Q$ is the measure for functional integration over all independent configurations of the order parameter, and $Z \equiv \int\mathcal{D}Q\exp(-F/k_BT)$ is the partition function. From this Ornstein-Zernicke form we identify a fluctuation correlation length

$$\xi(T) \equiv \sqrt{\frac{L_1}{a(T-T^-)}}, \tag{3.7}$$

which grows as the transition is approached from above. The fluctuations are isotropic, and would diverge as $k \to 0$ and as $T \to T^-$ from above. However, this divergence is preempted by the first-order transition at $T_{I\text{-}N} > T^-$.

IV. DYNAMICS OF FLUIDS OF NEMATOGENS

The equations of motion for flowing nematogens at temperatures near the equilibrium I-N transition temperature have been introduced previously by Hess [2], and subsequently in Ref. [3]. They are coupled equations of motion for the fluid velocity $\mathbf{v}(\mathbf{r},t)$ and the *entire* order parameter $Q_{\alpha\beta}(\mathbf{r},t)$, and may be regarded as generalizations of the Navier-Stokes and Leslie-Ericksen equations [22], enlarged to admit variations in the *amplitude* degrees of freedom of the order parameter, and hence biaxiality. Their derivation is presented in Refs. [2] and [3], and follows the standard strategy of nonequilibrium thermodynamics [35, 36]: (i) calculate the entropy production, starting from the assumption of local equilibrium, in accordance with the conservation of mass, energy, and linear and angular momentum; and (ii) make a linear Onsager expansion of the dissipative fluxes (i.e, the dissipative symmetric stress tensor, and the motion of the order parameter relative to the rotation of the fluid) in terms of the conjugate forces. For the sake of simplicity, we assume (i) that temperature gradients are negligible (i.e., that the thermal diffusivity is large), and (ii) that the fluid is incompressible, $\nabla\cdot\mathbf{v}=0$. Thus, we are restricting our attention to thermotropic liquid crystals. The description of lyotropic liquid crystals (i.e., solutions of rodlike molecules that exhibit nematic phases at sufficiently high concentrations) would necessarily be somewhat more elaborate, requiring the incorporation of concentration variations.

The coupled equations of motion for the fluid velocity and the order parameter are

$$\rho\,(\partial_t+\mathbf{v}\cdot\nabla)\,v_\alpha = \partial_\gamma\,\sigma_{\alpha\gamma}\,, \tag{4.1a}$$

$$(\partial_t+\mathbf{v}\cdot\nabla)\,Q_{\alpha\beta} = \kappa^{[a]}_{\alpha\gamma}Q_{\gamma\beta}-Q_{\alpha\gamma}\kappa^{[a]}_{\gamma\beta} +\beta_1\kappa^{[s]}_{\alpha\beta}+\frac{1}{\beta_2}H^{[s]}_{\alpha\beta}\,. \tag{4.1b}$$

The total stress tensor $\sigma_{\alpha\beta}$ includes an irreversible (i.e., dissipative) symmetric part $\sigma^{i[s]}_{\alpha\beta}$, an irreversible antisymmetric part (i.e., a torque) $\sigma^{i[a]}_{\alpha\beta}$, a reversible distortion part $\sigma^{d}_{\alpha\beta}$, and an isotropic pressure part $-p\,\delta_{\alpha\beta}$, and is given by

$$\sigma_{\alpha\beta} = \sigma^{i[s]}_{\alpha\beta}+\sigma^{i[a]}_{\alpha\beta}+\sigma^{d}_{\alpha\beta}-p\,\delta_{\alpha\beta}\,, \tag{4.2a}$$

$$\sigma^{i[s]}_{\alpha\beta} = \beta_3\kappa^{[s]}_{\alpha\beta}-\beta_1H^{[s]}_{\alpha\beta}\,, \tag{4.2b}$$

$$\sigma^{i[a]}_{\alpha\beta} = H^{[s]}_{\alpha\gamma}\,Q_{\gamma\beta}-Q_{\alpha\gamma}\,H^{[s]}_{\gamma\beta}\,, \tag{4.2c}$$

$$\sigma^{d}_{\alpha\beta} = -\frac{\delta F}{\delta\,\partial_\alpha Q_{\lambda\rho}}\,\partial_\beta Q_{\lambda\rho}\,. \tag{4.2d}$$

Here, $H_{\alpha\beta}\equiv-\delta F/\delta Q_{\alpha\beta}$ is the molecular field, β_1 is a dimensionless kinetic coefficient, β_2 and β_3 are positive viscosities, and the minus sign in Eq. (4.2b) conforms with Onsager reciprocity [35, 36]. The tensor field $\kappa_{\alpha\beta}\equiv\partial_\alpha v_\beta(\mathbf{r},t)$ is the velocity gradient tensor, and we use the notation $T^{[s]}_{\alpha\beta}$ and $T^{[a]}_{\alpha\beta}$ to denote the symmetric-traceless and antisymmetric portions of any tensor $T_{\alpha\beta}$.

The equations of motion, Eqs. (4.1a) and (4.1b), follow from the local entropy production density (i.e., the dissipation) ϑ, which is given by

$$T\vartheta = \Sigma_{\alpha\beta}\,H^{[s]}_{\alpha\beta}+\sigma^{i[s]}_{\alpha\beta}\,\kappa^{[s]}_{\alpha\beta}, \tag{4.3}$$

in which the flux $\Sigma_{\alpha\beta}$ is defined by

$$\Sigma_{\alpha\beta}\equiv(\partial_t+\mathbf{v}\cdot\nabla)\,Q_{\alpha\beta}-\left(\kappa^{[a]}_{\alpha\gamma}Q_{\gamma\beta}-Q_{\alpha\gamma}\kappa^{[a]}_{\gamma\beta}\right), \tag{4.4}$$

together with the linear Onsager expansion of the fluxes ($\Sigma_{\alpha\beta}$ and $\sigma^{i[s]}_{\alpha\beta}$) in terms of their conjugate forces ($\kappa^{[s]}_{\alpha\beta}$ and $H^{[s]}_{\alpha\beta}$):

$$\Sigma_{\alpha\beta} = \beta_1\kappa^{[s]}_{\alpha\beta}+\beta_2^{-1}H^{[s]}_{\alpha\beta}\,, \tag{4.5a}$$

$$\sigma^{i[s]}_{\alpha\beta} = \beta_3\kappa^{[s]}_{\alpha\beta}-\beta_1H^{[s]}_{\alpha\beta}\,. \tag{4.5b}$$

Using the resulting equations of motion, Eqs. (4.1a) and (4.1b), the local entropy production density may be expressed as

$$T\vartheta = \beta_3\kappa^{[s]}_{\alpha\beta}\kappa^{[s]}_{\alpha\beta}+\frac{1}{\beta_2}H^{[s]}_{\alpha\beta}H^{[s]}_{\alpha\beta}\,. \tag{4.6}$$

The distortion stress tensor $\sigma^{d}_{\alpha\beta}$ can be calculated from Eq. (4.2d) using the distortion free energy, Eq. (3.5), which yields

$$\sigma^{d}_{\alpha\beta} = -L_1\,\partial_\alpha Q_{\mu\nu}\,\partial_\beta Q_{\mu\nu}-L_2\,\partial_\beta Q_{\alpha\mu}\,\partial_\nu Q_{\nu\mu}\,. \tag{4.7}$$

(While this form of the distortion stress tensor is generally not symmetric, it becomes symmetric in the one-constant approximation.) The molecular field $H_{\alpha\beta}$ can

be calculated from the Landau–de Gennes and distortion free-energy densities, Eqs. (3.4) and (3.5), yielding

$$H_{\alpha\beta} = -A(T)\,Q_{\alpha\beta} - B\,Q_{\alpha\lambda}Q_{\lambda\beta} - C Q_{\alpha\beta}\,Q_{\lambda\rho}Q_{\lambda\rho} - L_1\,\nabla^2 Q_{\alpha\beta} - L_2\,\partial_\alpha\partial_\rho Q_{\rho\beta}\,. \tag{4.8}$$

It may be shown that under the constraint of uniaxial order, homogeneous in amplitude (i.e., $S_2 = 0$, and S_1 a spatially and temporally nonzero constant) the equations of motion (4.1a) and (4.1b) reduce, as they should, to the Leslie-Ericksen equations for director dynamics [37], provided the following correspondences between transport coefficients are made:

$$\beta_1 = 3S_1\,\lambda/2, \tag{4.9a}$$

$$\beta_2 = 2\gamma_1/(9S_1^2), \tag{4.9b}$$

$$\beta_3 = 2\,\nu_2\,. \tag{4.9c}$$

Here, the parameters of LE theory $\{\lambda, \gamma_1, \nu_2\}$ are, respectively, a ratio of rotational viscosities, a rotational viscosity, and the standard shear viscosity of the Navier-Stokes equation; see Ref. [27]. Notice that while the LE theory has five transport coefficients, only three appear in Eqs. (4.9a)–(4.9c). This discrepancy arises because the equations of motion (4.1a) and (4.1b) follow from an expansion in powers of $Q_{\alpha\beta}$; retention of higher orders in $Q_{\alpha\beta}$ would introduce additional transport coefficients. Consequently, it may be anticipated that our results are quantitatively self-consistent only when $Q_{\alpha\beta}$ is small, e.g., not far from the equilibrium I-N transition temperature. We also note that conventional LE theory is appropriate when the molecular field enforcing uniaxial order of fixed magnitude dominates the biaxial and ordering effects of flow (e.g., at sufficiently low temperatures and strain rates).

Related equations of motion have been derived from a microscopic model based on the rotational diffusion equation for the molecular orientation distribution function [7]. The resulting description depends on the following phenomenological parameters: (i) the rotational diffusion constant and (ii) a Maier-Saupe–like excluded-volume parameter. This description is, at present, limited to homogeneous states, although it may, in principle, be extended to inhomogeneous states by incorporating translational diffusion [38].

V. HOMOGENEOUS STATES

A variational (i.e., "effective free energy") approach to the description of the nonequilibrium states of fluids of nematogens in shear flow does not exist. We have therefore chosen to identify the candidate nonequilibrium phases by determining the stable stationary homogeneous states of the system in the absence of noise. This procedure is a nonequilibrium analog of the mean-field description of an equilibrium system, and should give us a qualitatively accurate description of the nonequilibrium phase diagram. Due to the absence of some analog of a thermodynamic potential, however, we shall have to resort to other means in order to select between candidate phases at locations in the nonequilibrium phase diagram where more than one such state exists. A discussion of the issue of state selection, and the consequent issue of coexistence, is postponed until Sec. VI; the subject of noise and fluctuations is postponed until Sec. VII.

A. Stationarity conditions for homogeneous states

We take stationary homogeneous states to be those states in which the thermodynamic fluxes $\Sigma_{\alpha\beta}$ and $\sigma^{i[s]}_{\alpha\beta}$ are stationary and homogeneous, i.e., independent of time and position. As a consequence of the Onsager expansion, Eqs. (4.5a) and (4.5b), their conjugate forces $\kappa^{[s]}_{\alpha\beta}$ and $H^{[s]}_{\alpha\beta}$ are also stationary and homogeneous. From Eq. (4.8) we see that the stationarity and homogeneity of $H^{[s]}_{\alpha\beta}$ implies the stationarity and homogeneity of $Q_{\alpha\beta}$. Then, from the definition of $\Sigma_{\alpha\beta}$, Eq. (4.4), we find the stationarity and homogeneity of $\kappa^{[a]}_{\alpha\beta}$.

We now turn to the coupled nonlinear partial differential equations for the velocity and order-parameter fields, Eqs. (4.1a) and (4.1b). As we have seen, stationary, homogeneous states satisfy $\partial_t Q_{\alpha\beta} = 0$, $\partial_t \kappa_{\alpha\beta} = 0$, $\partial_\gamma Q_{\alpha\beta} = 0$, and $\partial_\gamma \kappa_{\alpha\beta} = 0$. As we are focusing on bulk properties, we adopt periodic boundary conditions for $Q_{\alpha\beta}$ in all three directions, x, y, and z. Similarly, we adopt periodic boundary conditions for $\mathbf{v}$ in the x and z directions. However, in the y direction we impose "no-slip" boundary conditions, so that the fluid and the boundary plates move at the same velocity, which is directed in the x direction. Then, the homogeneity and stationarity of the velocity gradient, together with the constancy (in time) of the plate velocities and the boundary conditions on $\mathbf{v}$, require that v_y and v_z are zero throughout the fluid, and that v_x varies linearly with y but is independent of x and z. Thus $\mathbf{v}(\mathbf{r}) = D\,y\,\hat{\mathbf{x}}$, in which D is the stationary and homogeneous strain rate. Under these conditions, the equations of motion become nonlinear algebraic equations, coupling the strain rate D and nematic order parameter $Q_{\alpha\beta}$.

We wish to find solutions of these equations as functions of the temperature and *either* the shear stress applied to the fluid *or* (its nonequilibrium conjugate) the strain rate of the flowing fluid (and for appropriate physical choices of material parameters such as the Landau–de Gennes and Leslie coefficients). For ease of calculation we choose the latter option. Then, to find the stationary order-parameter configurations we need only consider the equation of motion for the order parameter, Eq. (4.1b). The velocity-field equation of motion, Eq. (4.1a), is automatically satisfied, because for the homogeneous states which we are considering the momentum flux density tensor $\partial_\beta(\sigma_{\alpha\beta} - \rho v_\alpha v_\beta)$ vanishes. Thus, we find numerically the stationary value (or values) of $Q_{\alpha\beta}$, and then compute the value of the shear stress necessary to maintain these states. By doing this, we construct two-dimensional surfaces of stationary states, in the space spanned by temperature, strain rate, nematic order parameter, and applied stress. As we shall see below, when we discuss inhomogeneous states, pairs of phases — if they do so — coexist at common values of their temperature and

stress, and not at common temperature and *strain rate*. Thus, for considering coexistence it is appropriate to analyze the states as functions of temperature and stress. However, for the intermediate purpose of considering the existence of homogeneous states it is simpler to consider the temperature and strain rate to be fixed. We remind the reader that the stress, strain rate, and nematic order parameter are related by Eq. (4.2b).

Let us then examine the stationarity condition for $Q_{\alpha\beta}$, in the presence of the planar shear flow $\mathbf{v}(\mathbf{r}) = D\,y\,\hat{\mathbf{x}}$. The director $\hat{\mathbf{n}}$ lies in the shear plane at an angle θ with respect to the flow, and the subdirector $\hat{\mathbf{m}}$ may also be taken to lie in the shear plane, as depicted in Fig. 2. (We will see, below, that this includes all locally stable homogeneous steady states.) Inserting the parametrization (3.2) in Eq. (4.1b), we find the following stationarity conditions:

$$\beta_1\beta_2 D\sin 2\theta = S_1\left[A(T) + \tfrac{1}{2}\left(3S_1^2 + S_2^2\right)\right] + \tfrac{1}{2}B\left(S_1^2 - \tfrac{1}{3}S_2^2\right), \tag{5.1a}$$

$$\beta_1\beta_2 D\sin 2\theta = \tfrac{1}{2}(S_1 - S_2)\left[A(T) + \tfrac{1}{2}C\left(3S_1^2 + S_2^2\right)\right] - \tfrac{1}{12}B\left(S_2^2 - 6S_1S_2 - 3S_1^2\right), \tag{5.1b}$$

$$2\,\beta_1\cos 2\theta = 3S_1 + S_2\,. \tag{5.1c}$$

These three conditions determine the magnitude of the two amplitudes S_1 and S_2, and the orientation of $\hat{\mathbf{n}}$ in the shear plane with respect to $\mathbf{v}$, as a function of the strain rate D and the temperature T, which enters through $A(T)$. The alignment condition (5.1c) is independent of strain rate, and is a generalization of the Leslie-Ericksen alignment condition $\cos 2\theta = \lambda^{-1}$ [22, 23].

B. Stationary states

In Ref. [3] we computed the stationary states for a fixed set of material parameters chosen to exemplify low-molecular-weight thermotropic nematogens, as a function of the dimensionless strain rate δ and the dimensionless temperature τ. We define these dimensionless parameters, along with the dimensionless applied shear stress s, through

$$\tau \equiv A(T)/C\,, \tag{5.2a}$$

$$\delta \equiv D\beta_2/C\,, \tag{5.2b}$$

$$s \equiv \sigma_{xy}/C\,. \tag{5.2c}$$

Now, in dimensionless form the stationarity conditions become

$$0 = \left[\hat{\kappa}^{[a]}_{\alpha\mu}Q_{\mu\beta} - Q_{\alpha\mu}\hat{\kappa}^{[a]}_{\mu\beta} + \beta_1\hat{\kappa}^{[s]}_{\alpha\beta}\right]\delta - \tau Q_{\alpha\beta} - \frac{B}{C}Q_{\alpha\lambda}Q_{\lambda\beta} - Q_{\alpha\beta}Q_{\lambda\rho}Q_{\lambda\rho} - \frac{B}{3C}\delta_{\alpha\beta}Q_{\lambda\rho}Q_{\lambda\rho}\,, \tag{5.3}$$

where $\hat{\kappa}_{\alpha\beta} \equiv \kappa_{\alpha\beta}/D$ is the dimensionless strain-rate tensor. In this form it is evident that the nature of the states is determined by only two material parameters: (i) the kinetic coefficient β_1 (which, by correspondence with LE theory, is a ratio of rotational viscosities [27]); and (ii) the ratio of Landau–de Gennes parameters B/C (which is a measure of the weakness of the first-order transition; recall that $\Delta S_1 = -2B/9C$). From a typical value of the order-parameter discontinuity at the equilibrium transition, $\Delta S_1 \sim 0.3$ [30], we have chosen $B/C = -1.2$. We have used $\beta_1 = 0.9$, which follows from the correspondence with LE theory, Eq. (4.9a), along with the reasonable value $\lambda \sim 2.0$ [27].

Figure 3 depicts stationary states through their values of S_1, i.e., the largest eigenvalue of $Q_{\alpha\beta}$, as a function of dimensionless temperature τ, for a particular value of the dimensionless strain rate δ. Dashed (solid) lines correspond to states which are unstable (stable) at fixed

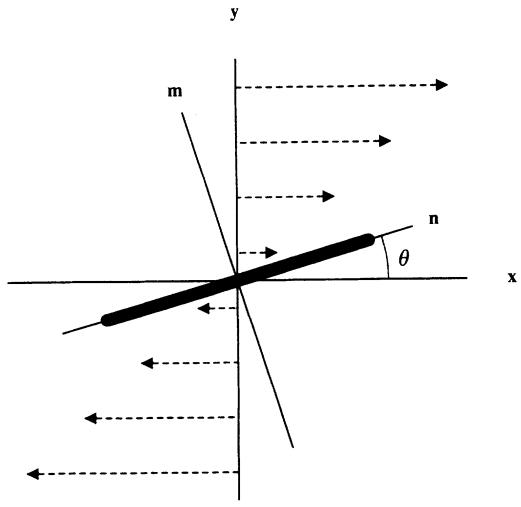

FIG. 2. Parametrization of homogeneous stationary states of nematic alignment in terms of the rotation of the director $\mathbf{n}$ with respect to the flow direction.

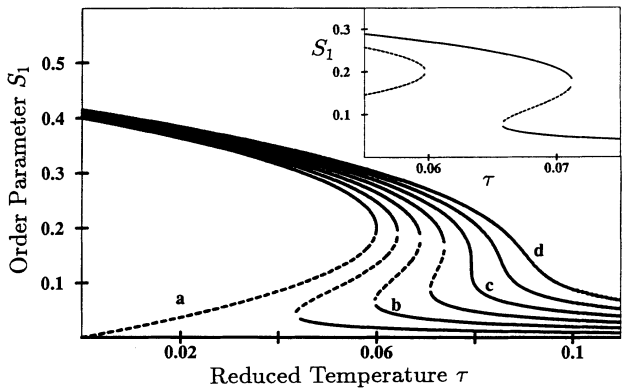

FIG. 3. Uniaxial order parameter S_1, as a function of reduced temperature τ, for branches containing the stable roots $Q_{\alpha\beta}$, for a range of values of the (dimensionless) strain rate and for material parameters $B = -1.2\,C$ and $\beta_1 = 0.9$: (a) $\delta = 0$; (b) $|\delta| < \delta_{\rm crit}$; (c) $|\delta| = \delta_{\rm crit}$; and (d) $|\delta| > \delta_{\rm crit}$. Dashed (solid) lines correspond to states which are unstable (stable) at fixed strain rate (but not necessarily at fixed stress; see Sec. V D). The inset shows all stationary values of S_1 for a dimensionless strain rate $\delta = 0.005$.

strain rate (but not necessarily at fixed stress; see below in Sec. V D). The stable order-parameter configurations have two principal axes (director and subdirector) in the shear plane, and the third orthogonal to it. (The shear plane is defined to be the plane containing both the fluid velocity and the gradient of the fluid speed; in the present case it is the xy plane.) At high temperatures there is a single stable state $Q^{+}_{\alpha\beta}$ available to the system, which is weakly ordered and has a relatively high degree of biaxiality. In fact, one may readily solve the stationarity conditions, Eqs. (5.1a)–(5.1c), in the limit of weak shear flow, $|D| \ll A(T)\,\beta_2$, to find that for the state $Q^{+}_{\alpha\beta}$

$$\theta(D,T) \simeq \frac{\pi}{4} - \frac{\beta_2}{4A(T)}|D| = \frac{\pi}{4} - \frac{1}{4\tau}|\delta|\,, \tag{5.4a}$$

$$S_1(D,T) \simeq -S_2(D,T) \simeq \frac{\beta_1\beta_2}{2A(T)}|D| = \frac{\beta_1}{2\tau}|\delta|\,. \tag{5.4b}$$

We have adopted the notation $Q^{+(-)}_{\alpha\beta}$ to signify the more (less) weakly ordered of two locally stable states, which is continuously connected to the high- (low-) temperature branch. As the temperature is reduced, a second state (as well as additional unstable states) becomes available to the system, and at still lower temperatures this new state becomes the only stable state. This new state $Q^{-}_{\alpha\beta}$ is well ordered and nearly uniaxial, reflecting the dominance, at lower temperatures, of the thermodynamic forces (i.e., the molecular field). In the limit of small strain rate, $|D| \ll A(T)\,\beta_2$, the corrections to the order parameter in the state $Q^{-}_{\alpha\beta}$ due to the flow are given by

$$S_1(D,T) \simeq S_0(T) + r\,|D|\,, \tag{5.5a}$$

$$S_2(D,T) \simeq -\left[B + 6S_0(T)C\right] r|D|/2B\,, \tag{5.5b}$$

where

$$r \equiv \frac{\sqrt{4\beta_1^2 - 9S_0(T)^2}}{\beta_2\, S_0(T)\left(B + 6S_0(T)\,C\right)}\,, \tag{5.5c}$$

$$S_0(T) \equiv -B/6C + \sqrt{2A(T)/3C}\,. \tag{5.5d}$$

Notice the tendency, as $S_0(T)$ increases, for r to become imaginary, signaling the onset of temporally oscillatory states [39]. Here $S_0(T)$ is the equilibrium (i.e., $D = 0$) value of the order parameter [30], and the alignment angle is given by the stationarity condition (5.1c). Thus, we see that the primary role of shear flow at low temperatures is to dictate the orientation of molecular alignment.

In the intermediate regime of temperatures, and for strain rates not too large, there are two locally stable homogeneous states. The issue of which, if either, of these two states is physically selected is taken up again in Sec. VI. As the strain rate is increased, we find the family of curves depicted in Fig. 3. For low strain rates the curves indicate a high-temperature weakly ordered phase which gives way to a two-state region at lower temperatures, and to a single well-ordered phase at still lower temperatures. However, for higher strain rates we find qualitatively different behavior. For dimensionless strain rates larger than a critical value the state of the system varies smoothly with temperature, and there is no transition. Finally, when the temperature is varied at the critical strain rate the system undergoes a continuous but singular transition from the high- to the low-temperature state. This phenomenology will survive the transformation from fixed strain rate to fixed shear stress. However, the precise quantitative location of the critical point will undergo a slight modification.

C. Stability conditions

We have constructed the two dimensional surface of stationary states in the space spanned by temperature, strain rate, nematic order parameter, and shear stress, as a function of temperature and strain rate. That the surface is two dimensional is a reflection of the fact that there are two control parameters. It is a straightforward matter to use Eq. (4.2b) to convert the result of this procedure so as to provide the surface of strain rate and order parameter as a function of temperature and stress. It will be particularly profitable to have made this transformation in the following section, when we discuss state selection and coexistence. The transformation is effected simply by regarding the surface of states in the space spanned by temperature, strain rate, order parameter, and stress as a surface of strain rate and order parameter as a function of temperature and stress.

We now address the issue of the local stability of the various stationary states with respect to homogeneous fluctuations at fixed temperature and stress. We do this by considering the dynamics of infinitesimal homogeneous variations in the nematic order parameter

$$\delta Q_{\alpha\beta}(t) \equiv Q_{\alpha\beta}(t) - Q^{(0)}_{\alpha\beta} \tag{5.6}$$

about the locally stable homogeneous steady states $Q^{(0)}_{\alpha\beta}$. We parametrize such fluctuations via the five amplitudes $\{\xi^i(t)\}_{i=1}^5$ of the expansion of $\delta Q_{\alpha\beta}(t)$ in terms of a convenient complete orthonormal set of five traceless symmetric tensors $\{e^i_{\alpha\beta}\}_{i=1}^5$, i.e.,

$$\delta Q_{\alpha\beta}(t) = \sum_{i=1}^{5} \xi^i(t)\, e^i_{\alpha\beta} \tag{5.7}$$

and collect these amplitudes in a five-component vector $\boldsymbol{\xi}$; details of this parametrization are given in Appendix A. (Note that a summation will not be implied over repeated latin superscripts.) One should envisage these homogeneous fluctuations as vectors $\boldsymbol{\xi}$ in the five-dimensional order-parameter space, with coordinates $\{\xi^i\}$. We focus on the dynamics of the fluctuations obtained by linearizing Eq. (4.1b) in the fluctuation $\delta Q_{\alpha\beta}$. In order to maintain constant homogeneous stress there is an accompanying variation in the strain rate, which is determined using Eqs. (4.2b) and (4.2c). Thus, we eliminate the strain-rate dependence in the nematic order-parameter fluctuation equation of motion, derived from Eq. (4.1b), in favor of dependence on the order parameter and the stress. Then, using the orthonormality of the basis, the fluctuation dynamics at constant temperature and stress becomes

$$\dot{\boldsymbol{\xi}} = -\mathbf{M}\cdot\boldsymbol{\xi} + O(\xi^2), \tag{5.8}$$

where M is the appropriate fluctuation matrix. Thus, when subjected to infinitesimal homogeneous variations, the normal-mode components of the locally stable states relax with rates determined by the eigenvalues of M. We do not consider this linear stability analysis to be complete. Rather, one should undertake a systematic analysis of stability, by considering the dynamics of inhomogeneous variations in $Q_{\alpha\beta}(\mathbf{r},t)$ and $\mathbf{v}(\mathbf{r},t)$, subject to appropriate boundary conditions which include the condition that the boundary velocity may vary so as to maintain constant applied stress.

D. Summary of locally stable stationary homogeneous states

When the surface of states that are stable with respect to homogeneous fluctuations at fixed temperature and stress is projected on to the stress-temperature plane the result is a phase diagram spanned by stress and temperature, shown later in Fig. 9, which is qualitatively similar to the strain-rate–temperature phase diagram of Ref. [3]. At each point in the shaded region we find two locally stable homogeneous states, as shown in Fig. 4. At a cusp at the point with dimensionless temperature τ^* and dimensionless stress s^* [69] on the boundary of the two-state region there is a nonequilibrium critical point.

There are several reasons why it is reasonable to refer to this point as a critical point. The first is topological. Consider a point in the two-state region of the temperature-stress phase diagram. This point has two distinct images in the surface of stable stationary states. Now transport this point in the phase diagram around a closed path. If the path encloses the critical point then one image is transported into the other. If the path does not enclose the critical point then the image is transported into itself. The second reason follows from the first: because the surface of states is continuous the critical point in the phase diagram can be circumnavigated by an arbitrarily short path. However, the inclusion or omission of such a short path from a longer path, passing near the critical point and ending in the two-state region,

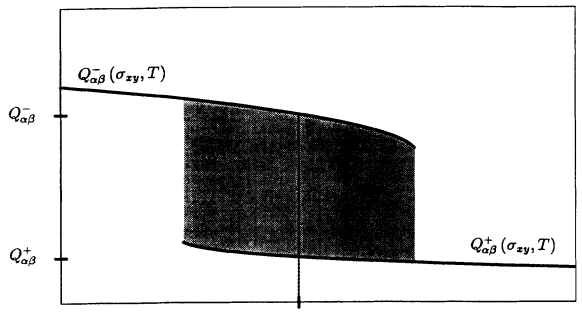

FIG. 4. Order parameter vs temperature for fixed applied stress. The branches labeled $Q^+_{\alpha\beta}(\sigma_{xy},T)$ and $Q^-_{\alpha\beta}(\sigma_{xy},T)$ are locally stable states. The shaded region is the two-state region, and the dotted line identifies the coexistence temperature as computed using the interface method described in Sec. VI). Due to the resolution of the plot, the turning points at the limits of stability do not appear.

leads to states which differ by a finite amount. Thus the dependence of the state on the temperature and stress is singular at this point. More physically, the dependence on temperature and stress of the strain rate, order parameter, and other quantities such as the effective viscosity, is singular in the vicinity of this point. Third, if state selection occurs on a certain coexistence line in the two-state region — and we shall find evidence that it does — then such a line would terminate at the critical point, thus providing the nonequilibrium analog of a line of first-order equilibrium phase transitions terminating in an equilibrium critical point. Fourth, at the critical point there is one particular mode of fluctuation, which is not a Goldstone mode, but which does not experience a linear restoring force and thus exhibits greater sensitivity to thermal noise. In the neighborhood of the critical point this mode undergoes anomalously large thermal fluctuations, and causes a nonequilibrium analog of (polarization-dependent) critical opalescence. All these features have their counterparts in equilibrium critical phenomena; it would be very useful to address the issues of nonlinear couplings between fluctuations, scaling, and criticality near this nonequilibrium critical point, and to explore the attendant issue of universality.

Using parameters reasonable for low-molecular-weight nematic fluids (such as MBBA [70]), i.e., $A = 50\ \mathrm{kJ\,m^{-3}K^{-1}}$, $B = -360\ \mathrm{kJ\,m^{-3}}$, $C = 300\ \mathrm{kJ\,m^{-3}}$, $\beta_1 = 0.9$, and $\beta_2 = 0.1\ \mathrm{kg\,m^{-1}\,s^{-1}}$, we find a critical value of the strain rate $D^* \sim 2 \times 10^5\ \mathrm{s^{-1}}$, and a temperature shift T^*–$T_{I\text{-}N} \approx 0.3\,\mathrm{K}$. While the magnitude of this strain rate is near the current limit of experimental feasibility, thus making observation of the critical point challenging, systems with a larger viscosity β_2 would have a more readily accessible critical strain rate. One example of such a system is the tobacco mosaic virus (TMV) in solution [40], which has rotational diffusion times one to two orders of magnitude larger than MBBA. As the TMV is a lyotropic system, a slightly more elaborate theoretical treatment, incorporating the presence of the solvent, is necessary. Alternatively, application of a magnetic field could help to bring the nonequilibrium critical point into a more readily accessible experimental regime.

We have discussed the construction of the phase diagram spanned by temperature and applied shear stress at some length. The reason for this is that coexistence, if it occurs, does so between states of fixed temperature and stress, as we shall discuss in Sec. VI. For a given stress σ_{xy}, we have found that there exist temperatures $T^+(\sigma_{xy})$ and $T^-(\sigma_{xy})$ between which the weakly ordered state (i.e., $Q^+_{\alpha\beta}$) and the strongly ordered state (i.e., $Q^-_{\alpha\beta}$) are both locally stable homogeneous states of the system. Thus, we must face the issues of state selection between, and coexistence of, nonequilibrium states.

Now, to choose which of two locally stable homogeneous *equilibrium* states is selected, e.g., near the first-order LG transition, one considers states with common values of temperature and pressure, and compares their chemical potentials. The state with the lower chemical potential is selected as the globally stable homogeneous equilibrium state. To locate where in the equilibrium phase diagram heterogeneous equilibrium may prevail,

i.e., where locally stable homogeneous states may coexist, one constructs the locus of points at which the chemical potentials of the homogeneous states are equal. This criterion follows from the equilibrium variational principle that the appropriate free energy be minimized, and allows one to identify the coexistence line [41]. It can be met in mean-field theory by Maxwell's "equal-area" construction.

It is natural, then, to enquire whether for our nonequilibrium system there is an intermediate temperature $T_{I\text{-}N}(\sigma_{xy})$, satisfying $T^{-}(\sigma_{xy}) \leq T_{I\text{-}N}(\sigma_{xy}) \leq T^{+}(\sigma_{xy})$ such that for temperatures $T > T_{I\text{-}N}(\sigma_{xy})$ the more weakly ordered state would be globally selected and for $T < T_{I\text{-}N}(\sigma_{xy})$ the more strongly ordered state would be globally selected, whereas at the temperature $T = T_{I\text{-}N}(\sigma_{xy})$ the two states could coexist. Such a temperature $T_{I\text{-}N}(\sigma_{xy})$ would play the same role out of equilibrium that a first-order transition temperature plays in equilibrium: it would provide the analog of a coexistence line, and the shaded region in Fig. 3 would then correspond to a region of metastability.

Although we postpone paying detailed attention to the question of global state selection until Sec. VI, what we can already say is that provided the steady homogeneous states that we have found are stable with respect to states that we have not yet considered, such as inhomogeneous (e.g., spatially modulated) steady states, and provided the system is not intrinsically hysteretic, with the ultimately selected state depending on the history of the system, then we can be certain that at some specific point within the two-state region (or possibly at its boundaries) the system makes a discontinuous transition between the homogeneous states available to it. If this is the case, then we may say that the system exhibits the nonequilibrium analog of a first-order phase transition.

Imagine attempting to increase the stress at fixed temperature across the nonequilibrium coexistence line. Then it is reasonable to conjecture that, on reaching the coexistence line, the steady state changes from the continuation of the homogeneous high-temperature phase, flowing with a low strain rate, to a phase-separated heterogeneous state in which high- and low-temperature (i.e., low- and high-strain-rate) states coexist. The relative fractions of the exhibited phases (and hence the location in real space of the interface between coexisting nonequilibrium states) are not determined by the control parameters, temperature and stress, alone; instead the net strain rate should be additionally specified. An analogous situation occurs at the LG transition, for which specification of a net volume is sufficient to determine the relative fractions of coexisting equilibrium liquid and gas phases. Upon attempting to increase the stress, the stress would in fact remain constant but the net strain rate would increase, as a progressively larger fraction of the system is converted into the continuation of the low-temperature phase. When the interface has swept across the system and the state has been entirely converted into the continuation of the low-temperature phase, the stress then increases and the system departs from the coexistence line. Of course, the kinetics — including analogs of metastability, nucleation, and spinodally controlled growth — of processes in such a nonequilibrium phase separation is an issue which must ultimately be considered, as must be the true singular nature of the physical properties in the vicinity of the critical point in which the nonequilibrium coexistence line terminates.

While there are many similarities between the stressed fluid of nematogens and the LG, we must bear in mind the significant differences, aside from the presence or absence of thermal equilibrium. In particular, the critical point in the flowing fluid of nematogens is a consequence of the suppression by flow of certain configurations in the five-dimensional nematic order-parameter space, while the LG critical point involves a scalar order parameter, namely the fluid density.

VI. INHOMOGENEOUS STATES: NONEQUILIBRIUM PHASE DIAGRAM, STATE SELECTION, COEXISTENCE, AND CRITICAL BEHAVIOR

A. State selection and coexistence away from equilibrium

Our identification of locally stable states has followed a mean-field approach: we have used deterministic equations of motion, and considered fluctuations only with regard to local stability. Next, we face the issue of choosing between a pair of locally stable steady states, i.e., the issue of global stability. In equilibrium this issue is resolved by comparing the chemical potentials of the relevant homogeneous states at common temperature and pressure: the state with the lower chemical potential is selected as the globally stable homogeneous equilibrium state, and the locus of points at which the chemical potentials are equal identifies the coexistence line. A corresponding variational principle has not been discovered for nonequilibrium thermodynamics, and in contrast with the equilibrium case we are unable to determine state selection and coexistence from an analysis of homogeneous states. While certain flows, such as uniaxial elongational flow, do admit a potential description [13, 25, 26, 42], general flows, and specifically the planar shear flows considered here, do not [43,44].

As we cannot appeal to a variational principle to determine which, if any, of a family of locally stable nonequilibrium states is globally and uniquely selected, we will take a more pragmatic approach. At applied stresses less than the critical value there is a range of temperatures for which there exist two locally stable homogeneous states; see Fig. 4. We wish to find which state, if either, is uniquely preferred at a particular temperature within this interval, and whether there is a temperature at which two phases may coexist. To address this issue we pick a fixed temperature and stress, and search for stationary stable inhomogeneous solutions of the equations of motion that interpolate between configurations which correspond to locally stable homogeneous phases. By using this "brute-force" method, we determine not only a coexistence line which, we conjecture, is a nonequilibrium analog of a line of equilibrium first-order transitions, but also information about the mean-field critical behavior

as the nonequilibrium critical point is approached [8].

In Ref. [3] we chose, as has commonly been done [7, 13, 26], to examine the nonequilibrium phase diagram with strain rate and temperature as independent variables. This procedure is adequate for identifying homogeneous phases but not, as we now discuss, for analyzing inhomogeneous states and issues of coexistence and criticality.

Recall that for an equilibrium isotropic fluid the pressures of coexisting phases must be equal in order to maintain a stationary interface; more generally, in the absence of any bulk forces (such as gravity) the pressure throughout any inhomogeneous state must be constant, so as to avoid macroscopic acceleration. In the nonequilibrium domain (and temporarily ignoring issues of stability) the condition analogous to equilibrium is that of stationarity (i.e., steadiness). In the present context of flowing nematogens, stationarity means that neither the velocity nor the order parameter may vary with time, i.e., $\partial_t \mathbf{v}(\mathbf{r},t) = \mathbf{0}$ and $\partial_t Q_{\alpha\beta}(\mathbf{r},t) = 0$. To maintain stationarity — in particular, for inhomogeneous states — it is necessary for the momentum flux density tensor to be homogeneous: $\partial_\gamma(\sigma_{\alpha\gamma} - \rho v_\alpha v_\gamma) = 0$ [45].

In order to address the issues of state selection and two-phase coexistence we have chosen to examine the next most general family of states beyond the homogeneous states. These are the states in which there is spatial variation only in the direction perpendicular to the boundary plates at which shear stress is applied, i.e., in the y direction. Thus, $Q_{\alpha\beta}(\mathbf{r},t) = Q_{\alpha\beta}(y)$ and $\mathbf{v}(\mathbf{r},t) = \mathbf{v}(y)$. The form of the velocity field may be further restricted by invoking incompressibility, which here reduces to $\partial_y v_y(y) = 0$. Then the boundary condition that the fluid not pass through the plates perpendicular to the y direction yields $v_y(y) = 0$. The additional boundary condition due to envisaged impenetrable boundary plates perpendicular to the z direction yields $v_z(y) = 0$. Thus, the velocity field remains directed along the x direction, the direction in which shear stress is applied, and we have $\mathbf{v}(\mathbf{r},t) = \hat{\mathbf{x}} \int_0^y dy' D(y')$, with $v_x(y)$ continuous. In the presence of these velocity and order-parameter fields the homogeneity of the momentum flux density tensor reduces to σ_{xy}, σ_{yy}, and σ_{zy} all spatially uniform, the values of the constants being determined by the forces applied at the boundary plates. Thus (i) σ_{yy} is adjusted to maintain the volume of the fluid; (ii) $\sigma_{zy} = 0$, because the shear stress is applied only in the x direction; and (iii) σ_{xy} is the equal and opposite force per unit area applied in the x direction to the boundary plates perpendicular to the y direction, as shown in Fig. 1. The stress σ_{xy} and the temperature T are the independent variables over which we envisage having experimental control, uniquely determining (except at coexistence) the state of the system. We will use the homogeneity of σ_{xy} to determine the order-parameter profile of inhomogeneous steady states.

Three remarks are in order here. First, we assume that the velocity of the boundary plates at which stress is applied is equal to the local velocity of the fluid. This "no-slip" boundary condition allows the computation of an effective macroscopic viscosity from the strain rate that results from a given applied shear stress. Second, we note that the precise steady-state condition associated with the temperature field is that the heat flux (rather than the temperature itself) be spatially and temporally constant, which permits variation in the temperature. However, for the sake of simplicity we have assumed that the thermal diffusivity is sufficiently large that the temperature variation is negligible. Third, if we were to ignore the structure of the interface between two homogeneous phases, and regard heterogeneous steady states as comprising a pair of homogeneous phases in contact at a planar interface perpendicular to the y axis, then the condition for thermal and mechanical equilibrium (necessary but not sufficient for coexistence) would be equality between the phases of their values of T, σ_{xy}, σ_{yy}, and σ_{zy}. This condition for equilibrium is the analog for anisotropic fluids of the equality of temperature and pressure, necessary (but not sufficient) for the coexistence of isotropic fluids. In equilibrium, state selection and coexistence are then determined by the chemical potentials of the states in question; out of equilibrium we shall determine these issues by using a numerical experiment.

B. Interface method for determining coexistence

To see if phase separation and coexistence do indeed occur in our system of nematogens in shear flow we impose boundary conditions on the order parameter in the y direction such that at one of the boundary plates it has the value found in one of the homogeneous stable states (associated with the given T and σ_{xy}), while at the other boundary plate it has the value found in the other homogeneous stable state. With the order parameter so constrained at the boundaries, we search for locally stable inhomogeneous states in which the order parameter and strain rate smoothly interpolate between the plates. From the nature of these interpolating states we infer the presence of a coexistence line, and locate its position in the nonequilibrium state diagram.

To illustrate this idea we first discuss a familiar equilibrium problem using this approach. Consider an Ising-like magnet in a small applied magnetic field h below its Curie temperature T_c. Using a coarse-grained description, the free energy of the equilibrium state may be taken to be [10]

$$F = \min_{\phi(\mathbf{r})} \int_V dV \{ \tfrac{1}{2} m\phi^2 + \tfrac{1}{4}\lambda\phi^4 - h\phi + \tfrac{1}{2}|\nabla\phi|^2 \}, \qquad (6.1)$$

where $m = m_o(T - T_c)$ and the real scalar field ϕ represents an average of the magnetization over a length scale large compared with the lattice spacing but small compared with the system size. With periodic boundary conditions and in zero field the candidate mean-field equilibrium states are $\phi^\pm = \pm(-m/\lambda)^{1/2}$ as they minimize F. For a small positive field $h > 0$, two local minima exist, at $\phi^\pm(h)$, but the state $\phi^+(h)$ has the lower free energy and is therefore the globally stable equilibrium state. As the field is reduced, a first-order transition occurs at $h_c = 0$, where the free energies of the states $\phi^\pm(h = 0)$ are equal.

We now discuss an alternative method, generalizable

to nonequilibrium systems, for determining the nature of the stable states of the system for $T < T_c$ and arbitrary homogeneous h. We would like to determine, as we did above by minimizing the free energy, the transition field h_c and the globally selected state for $h \neq h_c$. Consider a finite-sized, nonfluctuating, one-dimensional system, and imagine that the order parameter is specified to be $\phi^+(h)$ at one end of the system and $\phi^-(h)$ at the other end, necessitating at least one interface (i.e., "kink") somewhere within the system. We will determine the coexistence field for this system by examining the behavior of a kink. For a positive field, the configuration $\phi^+(h)$ has the lower free-energy density, so that the interface is forced towards the $\phi^-(h)$ wall, thus minimizing the total free energy; the converse happens for a negative field. Finally, for zero applied field the interface lies in the middle of the system. This provides a simple numerical scheme for determining the globally selected state (for $h \neq h_c$) and the coexistence field ($h_c = 0$). The above arguments were made for a finite system; for an infinite system we should find closely related results, the essential difference being that coexistence is determined by the existence of a family of neutrally stable equilibrium states generated by relocating the interface, rather than by its location at the sample midpoint [46]. (For finite systems with nonsymmetry-related coexisting phases the interface at coexistence will generally lie somewhere other than exactly in the middle. However, only at coexistence will the ratio of volumes of each phase tend to a finite and nonzero limit as the limit of large systems is taken.)

We now apply this procedure to the fluid of nematogens under shear flow. To do this, we consider a system of finite extent in the $\hat{\mathbf{y}}$ direction, at fixed homogeneous temperature and applied stress, and examine the behavior of the interface which interpolates between the two configurations $Q^{\pm}_{\alpha\beta}(\sigma_{xy}, T)$ which are the locally stable homogeneous states; see Fig. 5. The applied boundary stress σ_{xy} induces a velocity gradient $\partial v_x/\partial y = D(y)$. As the strain rate and the order parameter are related by the stress, Eq. (4.2b), they will vary in concert across the system so as to maintain the homogeneity of the stress (or, more precisely, the momentum flux density). We will only consider states which vary in the direction normal to the interface, thus ignoring interesting phenomena related to capillary waves on, and instabilities of, the interface. By using this interface technique we have identified the globally stable steady states and, hence, the full stress-temperature phase diagram, Fig. 9 [47].

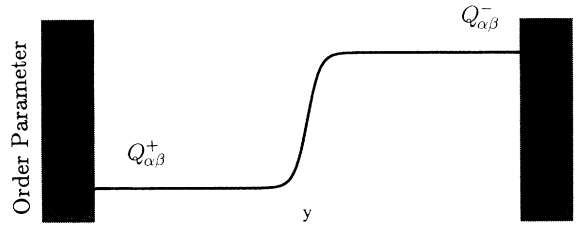

FIG. 5. Caricature of the order parameter vs spatial position y showing a stable interface at coexistence (four order-parameter dimensions have been suppressed). $Q^+_{\alpha\beta}$ refers to the order of the high-temperature state and $Q^-_{\alpha\beta}$ refers to the order of the low-temperature state.

C. Results of interface method

We have used the implicit Crank-Nicholson method [48] to find the stable interface profile, using an approach that correctly finds the stable steady states. However, the dynamics we have chosen to adopt for the relaxation are fictitious, because we have chosen to slave the velocity-field dynamics to the order parameter through the imposition of a homogeneous and constant stress tensor. In other words, in the relaxation scheme hydrodynamics is suppressed. We emphasize that the resulting inhomogeneous *steady states* are not sensitive to the choice of dynamics — all that is affected is the approach to these states (to which we are at present attaching no physical significance). For the majority of our computations we have chosen the parameters $B/C = -1.2$, $\beta_1 = 0.9$, $\beta_3/\beta_2 = 0.1$, and have used the approximation $L_1 = L_2 = L$. As shown in Ref. [37], this choice of the ratio β_3/β_2 is consistent with the correspondence with LE theory, Eqs. (4.9b) and (4.9c), along with typical experimental values $\gamma_1/\nu_2 \sim 2$ [49]. Experimentally, L_1 and L_2 are typically found to be roughly equal [30, 50]. Again, we use the dimensionless parameters, Eqs. (5.2a)–(5.2c), and measure lengths y and times t in dimensionless units $\bar{y}$ and $\bar{t}$ according to

$$\bar{t} \equiv tC/\beta_2, \tag{6.2a}$$

$$\bar{y} \equiv y\sqrt{C/L_1}. \tag{6.2b}$$

The position of the interface is characterized by a kink between the two stable configurations of the order parameter. As the order parameter has several components, we use the maximum of the distortion free-energy density as a scalar indicator of the kink location. As an exercise, we first performed this method for the ϕ^4 magnet and verified that we could determine state selection and coexistence at temperatures below the Curie point.

Using the interface method for the fluid of nematogens under shear stress we have located a coexistence line in the applied-stress–temperature plane for system sizes (in dimensionless units) 64, 128, and 256, with meshes of, respectively, 80, 80, and 160 points. Time steps were chosen in specific cases to find the stable states efficiently. For the larger two systems, on the order of 10^5 time steps were needed to achieve the stationary configuration.

D. Critical behavior

Figure 6 shows interface profiles at coexistence for the system of size 256, at reduced applied stresses $s = 0.0001, 0.0035$, and $0.003\,77$, which should be compared with the stress at the critical point, $(\tau^*, s^*) \simeq (0.081\,68, 0.003\,795)$ [51]. The interface is relatively sharp for small applied stress, and broadens as the stress approaches its critical value. This behavior is familiar from equilibrium systems, for which the width W of the interface between the two coexisting phases diverges like

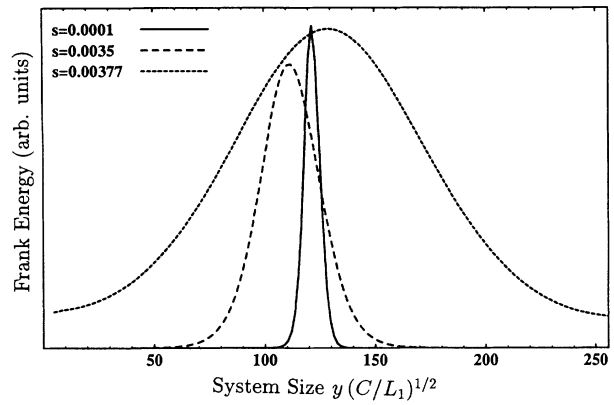

FIG. 6. Frank free-energy density profiles for interfaces at coexistence for a system of size $L = 256$ and for reduced applied stresses of $s = 0.0001$, 0.0035, and 0.003 77 for material parameters $B = -1.2C$, $\beta_1 = 0.9$, and $\beta_3 = 0.1\beta_2$. The critical point is located at $(\tau^*, s^*) \simeq (0.081\,68, 0.003\,795)$.

the correlation length, as the critical point is approached [52]. In equilibrium one expects the scaling law [14]

$$W \sim \xi \sim (T_c - T)^{-\nu}, \tag{6.3}$$

where ξ is the fluctuation correlation length and T_c is the equilibrium critical temperature. Within mean-field theory one expects $\nu = 1/2$. If we suppose that a diverging correlation length also emerges at the nonequilibrium critical point, then we expect a similar scaling law for the nematogenic fluid under stress. Figure 7 indicates scaling similar to classical equilibrium scaling, with $\nu \simeq 0.51 \pm 0.01$. We have defined W as the full width at half maximum of the distortion free energy, and verified that our results are robust with respect to this choice. We have also considered results for W from a sequence of systems of varying width, to ensure that our results are not artifacts of the finite system size. Using parameters typical of low-molecular-weight nematic fluids $(L/C \sim 10^4\,\text{Å}^2)$, we have found interface widths for small applied stress (i.e., near equilibrium) of a few

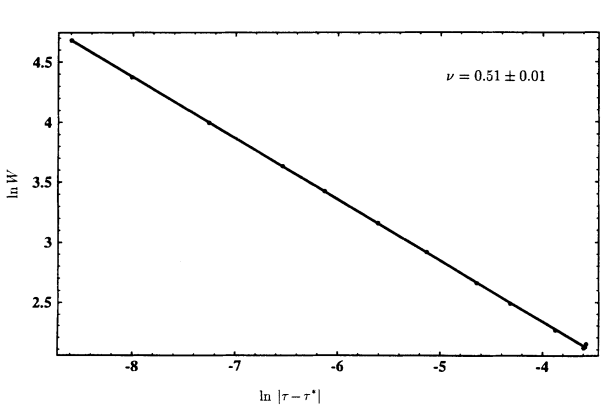

FIG. 7. $\ln W$ vs $\ln|\tau - \tau^*|$ for a system of size $L = 256$. The straight line indicates a best fit, corresponding to an exponent $\nu \simeq 0.51 \pm 0.01$.

100 Å, in reasonable agreement with the equilibrium nematic correlation length near the I-N transition [53].

A second scaling law concerns the behavior of the nematic order-parameter discontinuity along the coexistence curve, as the critical point is approached. In the LG the density difference along on the coexistence curve (i.e., the order parameter) scales as [54]

$$\rho_l - \rho_g \sim (T_c - T)^{\beta}, \tag{6.4}$$

where ρ_l and ρ_g are the densities of the coexisting liquid and gas phases. Within mean-field theory $\beta = 1/2$. Some care is needed to extend this type of scaling to the nematic order parameter $Q_{\alpha\beta}$ because of its multicomponent nature. Such a scaling relation characterizes the behavior of the particular mode in the system whose fluctuations have a diverging correlation length at the transition. In equilibrium, and within Landau mean-field theory, this critical mode is the mode whose quadratic coefficient in the effective free energy vanishes [11]. In a nonequilibrium system, we may define the critical mode as the mode whose fluctuations are long-lived (i.e., relax slower than exponentially) at the critical point. For the fluid of nematogens this mode is a certain linear combination of the five independent degrees of freedom of $Q_{\alpha\beta}$.

We identify the critical mode by considering the dynamics of an infinitesimal homogeneous fluctuation, $\delta Q_{\alpha\beta}(t) \equiv Q_{\alpha\beta}(t) - Q^{(0)}_{\alpha\beta}$, about the locally stable homogeneous steady state $Q^{(0)}_{\alpha\beta}$, Eq. (5.8), using the parametrization of Appendix A, just as we did in Sec. V C. The fluctuation matrix $\mathbf{M}$ is positive definite, except at the critical point, where we find a single zero eigenvalue whose eigenvector $\hat{\eta}$ corresponds to the slow mode. No symmetries remain to enforce eigenvalue degeneracies. For the nonequilibrium fluid of nematogens the (normalized) critical mode corresponds to a fluctuation along the direction

$$\hat{Q}_{\alpha\beta} = \sum_{i=1}^{5} \hat{\eta}^i\, e^i_{\alpha\beta}, \tag{6.5}$$

with $\hat{Q}_{\alpha\beta}\,\hat{Q}_{\alpha\beta} = 1$, which is (in principle) a linear combination of all five independent biaxial degrees of freedom. In practice, this critical mode corresponds to a combination of stretching the two amplitudes S_1 and S_2 (fluctuations along $e^1_{\alpha\beta}$ and $e^2_{\alpha\beta}$) and rotating the major director $\hat{\mathbf{n}}$ in the shear plane ($e^3_{\alpha\beta}$). For the choice of parameters $B = -1.2\,C, \beta_1 = 0.9$, and $\beta_3/\beta_2 = 0.1$, this massless mode is given by

$$\hat{Q}_{\alpha\beta} = 0.402\, e^1_{\alpha\beta} + 0.283\, e^2_{\alpha\beta} + 0.871\, e^3_{\alpha\beta}. \tag{6.6}$$

The next step is to characterize the *approach* to the nonequilibrium critical point along the coexistence line using a scalar order parameter, analogous to the density difference $(\rho_l - \rho_g)|_{T \to T_c}$ at LG coexistence. In the nonequilibrium fluid of nematogens, as one moves away from the critical point along the coexistence line, the order-parameter discontinuity grows and rotates (in order parameter space) away from the order parameter dif-

ference which first emerges at the nonequilibrium critical point, i.e., the critical mode. This rotation occurs because the alignment of the principal axes of $Q_{\alpha\beta}$ depends on the magnitude of order, and thus on the temperature and applied stress. To parametrize the vanishing of the critical mode at the critical point we use the magnitude of the projection of the order-parameter discontinuity $(Q^+_{\alpha\beta} - Q^-_{\alpha\beta})$ on to the critical mode $\widehat{Q}_{\alpha\beta}$, Eq. (6.6), measured along the coexistence line. Such a projection is implicit in the conventional analysis of the Heisenberg ferromagnet, for which the direction chosen for the magnetization by the spontaneously broken symmetry does not vary as the temperature continues to be reduced below the transition temperature. Since the inner product for the set $\{e^i_{\alpha\beta}\}$ is defined through a trace, we expect the following scaling relation, as the critical point is approached along the coexistence line:

$$(Q^+ - Q^-)_{\alpha\beta}\,\widehat{Q}_{\alpha\beta} \sim (\tau^* - \tau)^{\beta}. \tag{6.7}$$

Figure 8 shows a ln-ln plot of the projected order-parameter discontinuity versus the deviation $(\tau^* - \tau)$. As with the exponent ν, we find behavior suggestive of classical equilibrium criticality, namely $\beta \simeq 0.51 \pm 0.01$.

Although we do not have an "effective potential" description of this system, we may still understand the apparent classical behavior that we have recovered by examining the equation of motion for the critical mode. In addition to the vanishing of the mass term for the critical mode at the critical point, we find that the quadratic coefficient of the contribution of the critical mode to the equations of motion also vanishes. Hence, the structure is strongly reminiscent of the Landau mean-field theory for a scalar field near an equilibrium critical point [54]. This should not be too surprising: because we have omitted nonlinearly coupled fluctuations we should not expect to predict nonclassical critical behavior.

As a last remark on the singular temperature and stress dependence of the properties of the fluid of nematogens under shear flow, we note that we find a *single* critical mode. This suggests that the system has Ising-like critical behavior [14]. However, this scalar critical mode may be regarded as differing from that at conventional Ising-like critical points because it is a linear combination of both *amplitude* and *orientation* fluctuations, rather than a pure amplitude mode. In addition, the effects of advection and fluctuations must be included in order to determine whether the true critical behavior is or is not in fact classical [1]. These issues will be addressed, in part, in Sec. VII, when we return to the subject of fluctuations.

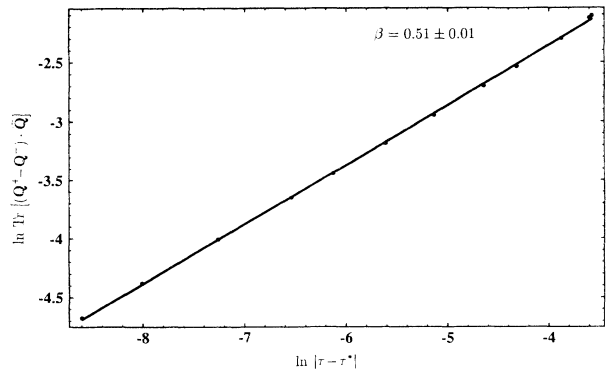

FIG. 8. $\ln \mathrm{Tr}\big[(\mathbf{Q}^+ - \mathbf{Q}^-)\cdot\widehat{\mathbf{Q}}\big]$ vs $\ln|\tau - \tau^*|$ for a system of size $L = 256$. The straight line indicates a best fit, corresponding to an exponent $\beta \simeq 0.51 \pm 0.01$.

E. Nonequilibrium phase diagram, coexistence, and critical phenomena

Figure 9 shows the complete nonequilibrium phase diagram in the (dimensionless) applied-stress versus temperature plane, including the coexistence line. This line interpolates smoothly between the equilibrium I-N transition and the nonequilibrium critical point. In addition to the nonequilibrium analogues of phenomena associated with equilibrium phase transitions and criticality, which we have discussed in detail (and collated in Table I), we conjecture that the nonequilibrium fluid of nematogens will exhibit phenomena analogous to the *nonequilibrium* phenomena commonly associated with first-order equilibrium transitions.

In particular, we conjecture that under careful control of, e.g., the temperature and applied stress it will be possible for the system to exhibit nonequilibrium metastability, so that it may be maintained for macroscopic times in the locally stable (i.e., nonsteady) but globally unstable state. In other words, we anticipate the possibilities of supercooling, superheating, superstressing, and substressing. In addition, for a decrease in temperature at fixed *strain rate*, we also expect the possibility of phase separation into regions differing in nematic order and strain rate, analogous to the phase separation of a fluid into a mixture of liquid and gaseous phases as, e.g., the temperature is decreased at fixed volume from the gaseous phase.

This nonequilibrium phase diagram has important rheological consequences. For fixed stress in the two-state re-

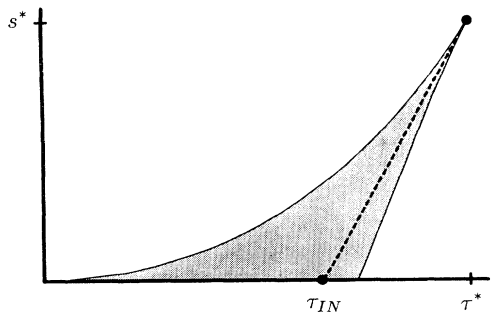

FIG. 9. Complete phase diagram in the reduced stress (s) vs reduced temperature (τ) phase diagram for material parameters $B = -1.2\,C$, $\beta_1 = 0.9$, $\beta_3 = 0.1\beta_2$, and $L_1/C = L_2/C = 10^4\ \text{Å}^2$. The dashed line represents the coexistence line; the shaded region is the two-state region with two locally stable states; the solid lines mark the limits of stability for the high- and low-temperature states. The nonequilibrium critical point is located at $(\tau^*, s^*) \simeq (0.0817, 0.003\,795)$.

TABLE I. Correspondence between phase transitions and critical phenomena for the equilibrium liquid-gas system and the nonequilibrium fluid of nematogens in shear flow.

Liquid-gas transition	Nematic in shear flow
Density ρ	Order parameter $Q_{\alpha\beta}$ or strain rate D
Temperature T	Temperature T
Pressure p	Stress σ_{xy}
Coexistence line in p-T plane	Coexistence line in $\sigma_{xy} - T$ plane
Liquid-gas phase separation	High-low strain-rate phase separation
Equilibrium critical point	Nonequilibrium critical point
Ising-like critical behavior	Critical amplitude and orientation mode $\widehat{\mathbf{Q}}$
$(\rho_l - \rho_g) \sim (T_c - T)^\beta$	$\mathrm{Tr}\,(\mathbf{Q}^+ - \mathbf{Q}^-) \cdot \widehat{\mathbf{Q}} \sim (T_c - T)^\beta$
Critical opalescence	Anomalous light scattering as $k \to 0$ for critical mode

gion, the state with the larger value of the order parameter flows with the larger strain rate and, correspondingly, has the smaller effective viscosity $\eta \equiv \sigma_{xy}/\partial_y v_x$. Hence, accompanying a discontinuity in the order parameter in the two-state region is also a discontinuity in the *strain rate*. Suppose, on the other hand, that the strain rate were prescribed rather than the stress. Then, for temperatures in the two-state region, it would be possible to select strain rates for which no homogeneous state is locally stable. The system would then respond by adopting an inhomogeneous state on the coexistence line, with the widths of the phase-separated fractions adjusted so as to obtain the selected strain rate, just as the equilibrium LG phase separates in order to exhibit a selected mean density.

The phase diagram for the fluid of nematogens under shear flow is topologically identical to that obtained for an equilibrium nematic with a positive magnetic susceptibility in the magnetic-field–temperature plane. There, one also finds a critical point for sufficiently strong fields [30]. Beyond the difference due to the equilibrium versus nonequilibrium nature of the applied fields, these critical points differ in symmetry, in the sense that the equilibrium transition occurs between identically oriented uniaxial phases, whereas the nonequilibrium transition (at least in shear flow) occurs between biaxial states, differing in both amplitudes and alignment. In addition, for equilibrium nematic states with a negative susceptibility a tricritical point is possible. Such a situation could also be realized for "disorientational" shear flows, i.e., flows which dictate a preferred plane for the director rather than a preferred axis [55].

Figure 9 shows the nonequilibrium phase diagram as a function of dimensionless temperature and shear stress. This figure, along with Fig. 3, displays several features reminiscent of the LG.

(i) The phase diagram of each system exhibits a line of discontinuous transitions which terminates with vanishing discontinuity in a critical point. For the LG the control parameters are, e.g., the temperature and the pressure, with the density exhibiting the discontinuity. For the nematogens in shear flow the control parameters are, e.g., the temperature and the shear stress, with the strain rate (and nematic order parameter, effective viscosity, etc.) exhibiting the discontinuity.

(ii) In the LG the system can be continuously transformed from one phase at a point on the coexistence curve to the other, through a sequence of homogeneous phases, by varying the external control parameters so as to circumnavigate the critical point. This is possible because the two phases have the same symmetry. For the same reason, such a continuous transformation is also possible between coexisting phases of the flowing nematogens, the symmetry of the phases being biaxial, due to the biaxiality of the shear stress.

(iii) In the nonequilibrium fluid of nematogens the quantities $\partial D/\partial T$, $\partial Q_{\alpha\beta}/\partial T$, etc., diverge as the critical point is approached at constant shear stress. Similarly, $\partial D/\partial \sigma_{xy}$, $\partial Q_{\alpha\beta}/\partial \sigma_{xy}$, etc., diverge as the critical point is approached at constant temperature. Thus, the differential viscosity $\partial \sigma_{xy}/\partial D$ vanishes in the neighborhood of the critical point. This divergence of $\partial D/\partial \sigma_{xy}$ is analogous to the divergence of the compressibility in the LG. Just as the LG exhibits divergent conjugate equilibrium fluctuations, i.e., density fluctuations, which cause critical opalescence and whose correlation length diverges, we anticipate analogous divergent strain-rate and order-parameter fluctuations which will cause polarization-dependent critical opalescence. Furthermore, we anticipate that the response to external magnetic fields of the nematic order parameter and strain rate will also be singular at the critical point. Such issues will be pursued in detail in Sec. VII, where we consider the role of thermal fluctuations.

We have now established, at a mean-field level, several substantial analogies between the I-N transition in shear flow and equilibrium systems such as the LG. In particular, there is a coexistence line ending in a critical point, at which there are singularities. Table I shows a more complete comparison of the two systems. In the next section we address fluctuations about the mean-field states, focusing on light-scattering experiments, which provide a direct probe of nematic fluctuations.

VII. FLUCTUATIONS IN FLUIDS OF NEMATOGENS UNDER SHEAR FLOW

We now turn to the subject of thermal fluctuations in fluids of nematogens under conditions of shear flow. In particular, we analyze the time dependence of linear inhomogeneous departures from stable stationary homogeneous states of the flowing nematic system, and discuss in detail two regimes of strain rate: (i) small strain rates, in order to explore the perturbative effect on equilibrium fluctuations and (ii) larger strain rates, near the critical strain rate, where anomalous nonequilibrium fluctuations lead to light scattering similar to that which characterizes critical opalescence at the LG critical point. In nematic fluids light is scattered by collective fluctuations of the nematic order parameter, which generate fluctuations of the dielectric tensor. Thus, by studying the scattering of light we should learn about order-parameter fluctuations

in fluids of nematogens in nonequilibrium states.

Let us first identify an important length scale which arises because of flow. Consider a fluctuation of spatial extent ℓ, having corresponding wave-number scale $k \sim 2\pi/\ell$. In flow two types of stress act to suppress this fluctuation: (i) elastic stress $\sigma_{\rm ela}$ associated with the deformation of the order parameter, which (at the level of the one-constant approximation) is

$$\sigma_{\rm ela} \sim L_1 \nabla^2 Q_{\alpha\beta} \sim L_1 k^2 Q_{\alpha\beta}\,, \tag{7.1}$$

and (ii) viscous stress $\sigma_{\rm vis}$ due to the velocity gradient which advects the fluctuation,

$$\sigma_{\rm vis} \sim \beta_2 (\partial_y v_x) \sim \beta_2 D, \tag{7.2}$$

where β_2 is a viscosity and D the strain rate. [Roughly speaking, these two stresses represent the forces in the order-parameter equation of motion, Eq. (4.1b).] These processes are of a comparable magnitude when the wave-number has the characteristic value

$$k_D \equiv \frac{2\pi}{\ell_D} \equiv \sqrt{\frac{D\beta_2}{L_1}}\,. \tag{7.3}$$

For fluctuations with $k \gg k_D$ the elastic restoring force dominates the dynamics, and correlations between fluctuations should essentially retain their equilibrium form. By contrast, the dynamics of fluctuations with $k \ll k_D$ is dominated by the viscous force, and we expect behavior which reflects the symmetry and advective effect of the flow.

A. Elastic light scattering from nematic states

Elastic light scattering from a uniaxial nematic state has been discussed extensively by many workers [50, 53, 56, 57]. However, because planar shear flow has biaxial symmetry, we will need to discuss scattering from a biaxial nematic state. We expand an arbitrary fluctuation about a nonequilibrium steady state, $\delta Q_{\alpha\beta}(\mathbf{r},t) \equiv Q_{\alpha\beta}(\mathbf{r},t) - Q^{(0)}_{\alpha\beta}$, in the convenient orthonormal basis $\{e^i_{\alpha\beta}\}$ (described in Appendix A) which represents kinematically independent fluctuations,

$$\delta Q_{\alpha\beta}(\mathbf{r},t) = \sum_{i=1}^{5} \xi^i(\mathbf{r},t)\, e^i_{\alpha\beta}\,. \tag{7.4}$$

We assume that the anisotropy of the dielectric tensor is determined by the order parameter of the anisotropic fluid, through the local relation [58]

$$\epsilon_{\alpha\beta}(\mathbf{r},t) = \bar{\epsilon}\,\delta_{\alpha\beta} + \mathcal{N} Q_{\alpha\beta}(\mathbf{r},t) + \cdots\,. \tag{7.5}$$

Omitted terms correspond to quantities built from other tensorial quantities, which may, in principle, affect the dielectric properties; examples include the temperature gradient $\partial_\alpha T$ and the stress $\sigma_{\alpha\beta}$. We assume that the stated contribution due to nematic order-parameter inhomogeneity dominates all other sources. As $\bar{\epsilon}$ is a homogeneous scalar, the fluctuations of the $\mathbf{k} \neq \mathbf{O}$ Fourier components of $\epsilon_{\alpha\beta}$ are proportional to the fluctuations of the order parameter,

$$\langle \delta\epsilon_{\alpha\beta}(\mathbf{k},t)\, \delta\epsilon_{\lambda\rho}(-\mathbf{k},t)\rangle = \mathcal{N}^2 \langle \delta Q_{\alpha\beta}(\mathbf{k},t)\, \delta Q_{\lambda\rho}(-\mathbf{k},t)\rangle. \tag{7.6}$$

The constant of proportionality $\mathcal{N}^2$ may be determined experimentally. The angle brackets denote an appropriate average, which in equilibrium would be an ensemble average with a Boltzmann weight for each microscopic state; out of equilibrium they denote an average over noise and initial conditions.

The differential cross section per unit solid angle for the elastic scattering of light through wave vector $\mathbf{k}$ is related to the fluctuations of the dielectric tensor of the fluid by [59]

$$\frac{d\sigma}{d\Omega} = \frac{\omega^4}{16\pi^2 c^4} \langle \delta\epsilon_{\alpha\beta}(\mathbf{k},t)\, \delta\epsilon_{\lambda\rho}(-\mathbf{k},t)\rangle\, \hat{p}_\alpha\, \hat{p}'_\beta\, \hat{p}_\lambda\, \hat{p}'_\rho\,, \tag{7.7}$$

where $\hat{\mathbf{p}}$ and $\hat{\mathbf{p}}'$ are, respectively, the polarization unit vectors of the incident and scattered light, and ω is the frequency of the light. Using Eqs. (7.4), (7.6), and (7.7), it is straightforward to calculate the scattering cross section in terms of the amplitude correlations $\langle \xi^i(\mathbf{k},t)\, \xi^j(-\mathbf{k},t)\rangle$:

$$\frac{d\sigma}{d\Omega} = \frac{\mathcal{N}^2\omega^4}{16\pi^2 c^4} \sum_{i,j=1}^{5} \langle \xi^i(\mathbf{k},t)\, \xi^j(-\mathbf{k},t)\rangle \times (\hat{p}_\alpha\, e^i_{\alpha\beta}\, \hat{p}'_\beta)\, (\hat{p}_\lambda\, e^j_{\lambda\rho} \hat{p}'_\rho). \tag{7.8}$$

Explicit results for four specific scattering and polarization geometries are given in Appendix C.

B. Steady-state correlations in nematic fluids under shear flow

The next step is to evaluate the nonequilibrium steady-state correlations of the fluctuations, $\langle \xi^i(\mathbf{k})\, \xi^j(-\mathbf{k})\rangle$, i.e., the long-time limit of the equal-time correlations $\langle \xi^i(\mathbf{k},t)\, \xi^j(-\mathbf{k},t)\rangle$, from which the sensitivity to (the distribution of) initial conditions has decayed away. In principle, $\langle \xi^i(\mathbf{k},t)\, \xi^j(-\mathbf{k},t)\rangle$ should be obtained from stochastic versions of the equations of motion for the order parameter and the fluid velocity, Eqs. (4.1b) and (4.1a), subject to appropriate boundary conditions on — *inter alia* — the velocity field (no slip) and the xy component of the stress. The boundary stress would then serve as a control parameter, along with temperature, and to provide fluctuations the equations would be augmented by noise terms. For the purpose of discussing fluctuations, however, we instead restrict our attention to states of nonfluctuating homogeneous strain rate D. Formally, this corresponds to a particular choice of noise in the ideal Langevin description, for which the order-parameter noise and stress noise are correlated such that there are no velocity-field fluctuations. This choice is made solely to ease the analysis: treating the velocity field as prescribed, homogeneous and immutable, and considering only the stochastic dynamics of the order-parameter field, produces considerable simplification, while continuing — we hope — to capture the essence of the physics.

Thus, we consider plane shear flow $\mathbf{v}(\mathbf{r}) = D\, y\, \hat{\mathbf{x}}$. The stable steady states for nonzero strain rate have the director $\hat{\mathbf{n}}$ in the shear plane (canted with respect to the flow direction) and the subdirector $\hat{\mathbf{m}}$ also in the shear plane,

reflecting the biaxiality induced by the shear flow. The equations of motion for the fluctuation $\delta Q_{\alpha\beta}$ are found by expanding Eqs. (4.1b) about the steady-state value for $Q_{\alpha\beta}$, which leads to a set of nonlinear equations of motion for $\delta Q_{\alpha\beta}$. We truncate the terms beyond linear order, thus treating the system within the nonequilibrium equivalent of the Gaussian approximation [10]. Next, we introduce noise into these equations to represent the coupling between the coarse-grained degrees of freedom that we are explicitly considering and the residual microscopic degrees of freedom. This noise encourages the system to probe configurations other than the homogeneous stable stationary states.

By expanding $\delta Q_{\alpha\beta}$ according to Eq. (7.4), projecting Eqs. (4.1b) on to the basis set $\{e^i_{\alpha\beta}\}$, and linearizing with respect to $\delta Q_{\alpha\beta}$, we obtain the following equation of motion for the five-component amplitude vector $\boldsymbol{\xi}(\mathbf{r},t)\,(=\{\xi^i(\mathbf{r},t)\})$:

$$(\partial_t + Dy\partial_x)\,\boldsymbol{\xi}(\mathbf{r},t) = -\beta_2^{-1}\,\Theta(-i\boldsymbol{\nabla})\cdot\boldsymbol{\xi}(\mathbf{r},t) + \boldsymbol{\zeta}(\mathbf{r},t), \tag{7.9}$$

where the 5×5 fluctuation matrix operator $\Theta(-i\boldsymbol{\nabla})$ is given by

$$\Theta(-i\boldsymbol{\nabla}) = \mathbf{M} - L_1\mathbf{I}\nabla^2, \tag{7.10}$$

in terms of the *mass matrix* $\mathbf{M}$, to be described shortly, and the *distortion matrix operator* $L_1\nabla^2\mathbf{I}$, in which $\mathbf{I}$ is the 5×5 identity matrix. Notice that as a consequence of the one-constant approximation (i.e., $L_2 = 0$; see the discussion in Sec. III B) the distortion matrix operator is isotropic in both real space and order-parameter space.

The Langevin noise source $\boldsymbol{\zeta}(\mathbf{r},t)$ in Eq. (7.9) is chosen to obey Gaussian statistics, with mean zero and variance chosen to satisfy the fluctuation-dissipation theorem (FDT) [60],

$$\langle\zeta^i(\mathbf{r},t)\,\zeta^j(\mathbf{r}',t')\rangle = 2k_{\mathrm{B}}T\,\beta_2^{-1}\,\delta^{ij}\,\delta(\mathbf{r}-\mathbf{r}')\,\delta(t-t'). \tag{7.11}$$

Invoking the FDT under the present circumstances requires some discussion. Our choice of noise ensures that in the *absence* of flow the stationary distribution function for the state will be the Boltzmann distribution [60]. Our assumption, then, is that the noise in the *driven* system obeys the same distribution as that in the same system *relaxing* to equilibrium. It is a nontrivial assumption. However, there do exist physical situations in which predictions based on the validity of the FDT for nonequilibrium steady states have been verified experimentally; an example is the series of light-scattering experiments on a fluid driven out of equilibrium by a stationary temperature gradient [61].

The mass matrix $\mathbf{M}$ is found to have the block structure

$$\mathbf{M} = \begin{pmatrix} \mathbf{M}^{(123)} & \mathbf{O} \\ \mathbf{O} & \mathbf{M}^{(45)} \end{pmatrix}, \tag{7.12}$$

where the 3×3 sector is given by

$$\mathbf{M}^{(123)} = \begin{pmatrix} A(T)+BS_1+\frac{1}{2}C(9S_1^2+S_2^2) & S_2\sqrt{3}\,(CS_1-\frac{1}{3}B) & -\sqrt{3}\,\beta_2 D \\ S_2\sqrt{3}\,(CS_1-\frac{1}{3}B) & A(T)-BS_1+\frac{3}{2}C(S_1^2+S_2^2) & \beta_2 D \\ \sqrt{3}\,\beta_2 D & -\beta_2 D & A(T)+\frac{1}{2}B(S_1+S_2)+\frac{1}{2}C(3S_1^2+S_2^2) \end{pmatrix} \tag{7.13}$$

and the 2×2 sector is given by

$$\mathbf{M}^{(45)} = \begin{pmatrix} A(T)+\frac{1}{2}B(S_1-S_2)+\frac{1}{2}C(3S_1^2+S_2^2) & -\beta_2 D \\ \beta_2 D & A(T)-BS_1+\frac{1}{2}C(3S_1^2+S_2^2) \end{pmatrix}. \tag{7.14}$$

The matrix $\mathbf{O}$ is an appropriately dimensioned matrix of zeros. The amplitudes S_1 and S_2 in the mass matrix characterize the stable homogeneous steady state in question, obtained in the absence of noise, and depend on (i) the Landau–de Gennes parameters $A(T)$, B, and C; (ii) the transport coefficients β_1 and β_2; and (iii) the strain rate D; see Eqs. (5.1a)–(5.1c). The block structure results from the fact that the principal axes of the order-parameter and strain-rate tensors have one common axis, namely the normal to the shear plane. The 3×3 block involves fluctuations in the amplitudes S_1 and S_2 and the orientation of the director *in* the shear plane, while the 2×2 block involves tilts of the director and the subdirector *out* of the shear plane. Notice that the effect of shear flow is to introduce both symmetric and antisymmetric off-diagonal contributions to $\mathbf{M}$, thus coupling the components of $\boldsymbol{\xi}(\mathbf{r},t)$, in addition to modifying the diagonal terms. (We remind the reader that $S_2 = 0$ when $D = 0$.) Thus, Θ is not integrable (i.e., it cannot be written as a second functional derivative), which is a reflection of the fact that shear flow does not admit an "effective free-energy" formulation.

For the sake of orientation we examine, in passing, the mass matrix for the uniaxial equilibrium state in the absence of shear, for which $Q_{\alpha\beta}$ is given by Eq. (3.2), with $S_1(T) = \theta^H(T_{I\text{-}N}-T)\,S_0(T)$ and $S_2(T) = 0$, in which $S_0(T)$ is given by Eq. (5.5d), and where θ^H is the usual Heaviside step function. For this state, and for $T > T_{I\text{-}N}$, the elements of the mass matrix $\mathbf{M}$ reduce to

$$M^{ij} = A(T)\,\delta^{ij}. \tag{7.15}$$

On the other hand, for $T < T_{I\text{-}N}$ the only nonvanishing elements of $\mathbf{M}$ are

$$M^{11} = -2A(T) - \tfrac{1}{2}BS_0(T)\,,$$
$$M^{22} = -\tfrac{3}{2}BS_0(T)\,, \qquad (7.16)$$
$$M^{55} = -\tfrac{3}{2}BS_0(T)\,.$$

The vanishing, for $T < T_{I\text{-}N}$, of M^{33} and M^{44} indicates the presence of Goldstone director fluctuations corresponding to the modes $e^3_{\alpha\beta}$ and $e^4_{\alpha\beta}$ (defined in Appendix A).

Now, our goal is to calculate steady-state correlations among the amplitudes $\{\xi^i(\mathbf{r},t)\}$. The dynamic correlations are also readily obtained and will be presented in a forthcoming calculation [62]. To do this we follow the technique used by OK [1], and subsequently Cates and Milner [5], who investigated the effect of shear flow on, respectively, the LG and I-L transitions. The starting point is the statement that the *stationary* equal time amplitude-amplitude correlation function $\chi^{ij}(\mathbf{k},t) \equiv \langle \xi^i(\mathbf{k})\xi^j(-\mathbf{k})\rangle_t$ satisfies

$$\partial_t\, \chi^{ij}(\mathbf{k},t) = 0\,, \qquad (7.17)$$

and the identification of $\boldsymbol{\chi}(\mathbf{k})$ as the stationary value of $\boldsymbol{\chi}(\mathbf{k},t)$. From the stochastic equation of motion for $\boldsymbol{\xi}(\mathbf{r},t)$ and the properties of the noise distribution we obtain the Fokker-Planck equation [60] for the normalized probability distribution functional $\mathcal{P}_t\{\boldsymbol{\xi}\}$ [63],

$$\partial_t\, \mathcal{P}_t\{\boldsymbol{\xi}\} = \int d^3r \sum_{i=1}^{5} \frac{\delta}{\delta\xi^i(\mathbf{r})} \left\{ \left[\frac{k_{\mathrm{B}}T}{\beta_2} \frac{\delta}{\delta\xi^i(\mathbf{r})} - \sum_{j=1}^{5} \left[D\, y\, \delta^{ij}\, \partial_x + \Theta^{ij}(-i\nabla) \right] \xi^j(\mathbf{r}) \right] \mathcal{P}_t\{\boldsymbol{\xi}\} \right\}. \qquad (7.18)$$

Averages over quantities at time t are calculated using $\langle \mathcal{O} \rangle_t = \int \mathcal{D}\boldsymbol{\xi}\, \mathcal{P}_t\{\boldsymbol{\xi}\}\, \mathcal{O}\{\boldsymbol{\xi}\}$, and the time evolution of averaged quantities is governed by $\partial_t \langle \mathcal{O} \rangle_t = \int \mathcal{D}\boldsymbol{\xi}\, \mathcal{O}\{\boldsymbol{\xi}\}\, \partial_t\, \mathcal{P}_t\{\boldsymbol{\xi}\}$. Here $\int \mathcal{D}\boldsymbol{\xi}$ indicates functional integration over the independent coarse-grained degrees of freedom, namely the amplitudes $\boldsymbol{\xi}(\mathbf{r})$. By using the Fokker-Planck equation and enforcing the stationary condition (7.17), we obtain the differential equation

$$Dk_x \frac{\partial}{\partial k_y} \boldsymbol{\chi}(\mathbf{k}) - \left\{ \Theta(k)\, \boldsymbol{\chi}(\mathbf{k}) + \boldsymbol{\chi}(\mathbf{k})\, \Theta^{\mathrm{T}}(k) \right\} = -\frac{2k_{\mathrm{B}}T}{\beta_2}\, \mathbf{I}\,, \qquad (7.19)$$

satisfied by the stationary correlations $\boldsymbol{\chi}(\mathbf{k})$, in which $\left(\Theta^{\mathrm{T}}\right)^{ij} \equiv \Theta^{ji}$.

Integrating Eq. (7.19) is a straightforward matter (described in Appendix B) which gives

$$\boldsymbol{\chi}(\mathbf{k}) = \beta_2^{-1}\, k_{\mathrm{B}}T \int_0^\infty dt \exp\left\{ -\beta_2^{-1} L_1 \int_0^t ds\, f(\mathbf{k}, Dk_x s/2) \right\} \exp\{ -\beta_2^{-1} \mathbf{M}\, t/2 \} \exp\{ -\beta_2^{-1} \mathbf{M}^{\mathrm{T}}\, t/2 \}\,, \qquad (7.20)$$

where $f(\mathbf{k},p) \equiv k_x^2 + (k_y+p)^2 + k_z^2$. In obtaining this result we have made use of the essential feature that, by virtue of the one-constant approximation to the distortion free energy, the fluctuation matrix operator, Eq. (7.10), commutes with itself at different values of the wave-vector magnitude, i.e., $[\Theta(k), \Theta(k')] = \mathbf{O}$. In fact, this result for $\boldsymbol{\chi}(\mathbf{k})$ could have been obtained with equal ease from the direct integration of the linear stochastic equation of motion, Eq. (7.9).

In order to simplify the expression for $\boldsymbol{\chi}(\mathbf{k})$ we next assume that $\mathbf{M}$ is diagonalizable by an invertible transformation matrix $\mathbf{U}$ [64]. If this is the case then $\mathbf{M}^{\mathrm{T}}$ is also diagonalizable, possessing the same set of eigenvalues, and we have

$$\mathbf{U}\, \mathbf{M}\, \mathbf{U}^{-1}\big|^{ij} = \left(\mathbf{U}^{\mathrm{T}}\right)^{-1} \mathbf{M}^{\mathrm{T}}\, \mathbf{U}^{\mathrm{T}}\big|^{ij} = m^i\, \delta^{ij}. \qquad (7.21)$$

[Recall that summation convention is *not* implied for our five-dimensional latin superscripts; thus the index i in Eq. (7.21) is not to be summed.] We refer to the eigenvalues $\{m^i\}$ as the *masses* of the fluctuation modes. By diagonalizing the last two factors in Eq. (7.20) via the insertion $\mathbf{I} = \mathbf{U}\mathbf{U}^{-1}$, and performing the s integration in the exponent, we obtain

$$\chi^{ij}(\mathbf{k}) = \sum_{k,l=1}^{5} \Gamma^{ij,\,kl} J^{kl}(\mathbf{k}), \qquad (7.22)$$

where

$$J^{kl}(\mathbf{k}) \equiv \frac{k_{\mathrm{B}}T}{\beta_2} \int_0^\infty dt \exp\left\{ -\frac{t(m^k + m^l + 2L_1 k^2)}{2\beta_2} - \frac{D^2 t^2}{2} \frac{k_x k_y}{k_D^2} - \frac{D^3 t^3}{12} \frac{k_x^2}{k_D^2} \right\}, \qquad (7.23)$$

in which k_D is the characteristic wave-vector set by the strain rate, Eq. (7.3), and

$$\Gamma^{ij,kl} \equiv \left(\mathbf{U}^{-1}\right)^{ik} \left(\mathbf{U}\mathbf{U}^{\mathrm{T}}\right)^{kl} \left[\left(\mathbf{U}^{\mathrm{T}}\right)^{-1} \right]^{lj}. \qquad (7.24)$$

(We remind the concerned reader that $\mathbf{M}$ is not symmetric, so that $\mathbf{U}$ is not orthogonal, $\mathbf{U}\mathbf{U}^{\mathrm{T}} \neq \mathbf{I}$.)

From the structure of $J^{kl}(\mathbf{k})$ we see that shear flow very strongly damps steady-state correlations, except for modes for which $k_x = 0$. In this special case, fluctuations are elongated parallel to the streamlines of the flow; heuristically we do not expect advection by shear flow to destroy these fluctuations. On the other hand, fluctuations whose wave vectors intersect streamlines (for which $k_x \neq 0$) have their correlations greatly reduced; see Fig. 11. Such wave-vector-dependent suppression is a general feature of fluctuations in shear flow, and is also seen in the binary fluid [1], the isotropic-lamellar transition [5], and the nematic–to–smectic-A transition [4]. Next we examine the behavior of light scattering for specific situations.

C. Light scattering near the equilibrium transition

1. Zero strain rate

We first examine the case of zero strain rate. In this case $\mathbf{M}$ is already diagonal [see Eqs. (7.15) and (7.16)] so that $\mathbf{U} = \mathbf{I}$, and Eq. (7.23) may be integrated exactly, yielding the familiar Ornstein-Zernicke form for scattering from a uniaxial nematic, Eq. (3.6),

$$\chi^{ij}(k)\big|_{D=0} = \frac{2k_BT}{m^i + m^j + 2L_1k^2} \,. \tag{7.25}$$

Of particular interest is the case $T < T_{I\text{-}N}$, for which the correlations $\chi^{33} = \chi^{44} = 1/(L_1k^2)$, representing anomalous director fluctuations. These may be most efficiently probed by considering, e.g., polarizations $\hat{\mathbf{p}} = \hat{\mathbf{n}}$ and $\hat{\mathbf{p}}' \perp \hat{\mathbf{n}}$, whence, from Eqs. (A3) and (7.8),

$$\left.\frac{d\sigma}{d\Omega}\right|_{D=0} \sim \langle|\xi^3(\mathbf{k})|^2\rangle \sim \frac{1}{L_1k^2} \quad (T < T_{I\text{-}N}). \tag{7.26}$$

For $T > T_{I\text{-}N}$ all masses are identical [Eq. (7.15)], and we expect isotropic scattering of the form $d\sigma/d\Omega \sim [a(T - T^-) + L_1k^2]^{-1}$, regardless of polarization.

2. Weak shear flow

Next we find the leading corrections to Eq. (7.25) in the regime of weak shear flow, which is defined by $(k/k_D)^2 \gg |\hat{k}_x|$, or equivalently $D \ll L_1k^2/\beta_2|\hat{k}_x|$. In this limit we may approximate $J^{kl}(\mathbf{k})$, Eq. (7.23), by

$$J^{kl}(\mathbf{k}) \simeq \frac{2k_BT}{m^k + m^l + 2L_1k^2}\left[1 - \frac{4L_1^2|\hat{k}_x||\hat{k}_y|k^2k_D^2}{(m^k + m^l + 2L_1k^2)^2} - \frac{4L_1^3\hat{k}_x^2\,k^2k_D^4}{(m^k + m^l + 2L_1k^2)^3} + \cdots\right], \tag{7.27}$$

in which we have retained only the leading corrections to the $D = 0$ limit. To obtain the correlation function $\boldsymbol{\chi}(\mathbf{k})$, we diagonalize the mass matrix $\mathbf{M}$, and express $\boldsymbol{\chi}(\mathbf{k})$ as a sum of contributions of correlations $J^{kl}(\mathbf{k})$ of the eigenmodes. Then there are two cases to consider.

(i) For $T < T_{I\text{-}N}(D)$ the stationarity conditions are given by Eqs. (5.5a) and (5.5b), from which we find the mass matrix

$$\mathbf{M} = \mathbf{M}^{(0)} + \mathbf{M}^{(1)}D + O(D^2). \tag{7.28}$$

Here, $\mathbf{M}^{(0)}$ is given by Eq. (7.16) and $\mathbf{M}^{(1)}$ is given by

$$\mathbf{M}^{(1)} = \begin{pmatrix} \mathbf{M}^{(1A)} & \mathbf{O} \\ \mathbf{O} & \mathbf{M}^{(1B)} \end{pmatrix}, \tag{7.29}$$

in which the submatrices $\mathbf{M}^{(1A)}$ and $\mathbf{M}^{(1B)}$ are given by

$$\mathbf{M}^{(1A)} = \begin{pmatrix} [B + 9CS_0(T)]\,r & \sqrt{3}\,[CS_0(T) - \frac{1}{3}B]\,\tilde{S}_2 & -\sqrt{3}\beta_2 \\ \sqrt{3}\,[CS_0(T) - \frac{1}{3}B]\,\tilde{S}_2 & -[B - 3CS_0(T)]\,r & \beta_2 \\ \sqrt{3}\beta_2 & -\beta_2 & \frac{3}{4}[B - 3CS_0(T)]\,r \end{pmatrix}, \tag{7.30a}$$

$$\mathbf{M}^{(1B)} = \begin{pmatrix} \frac{1}{4}[B - 3CS_0(T)]\,r & -\beta_2 \\ \beta_2 & -[B - 3CS_0(T)]\,r \end{pmatrix}. \tag{7.30b}$$

The quantity $\tilde{S}_2$ is given by

$$\tilde{S}_2 \equiv \lim_{D\to 0} S_2/D = -\frac{\sqrt{4\beta_1^2 - 9S_0^2}}{2\beta_2 BS_0}, \tag{7.31}$$

independent of D, and r is given by Eq. (5.5b). To first order in perturbation theory in D, we diagonalize $\mathbf{M}$ and construct the transformation matrix $\mathbf{U}$. Then, from Eq. (7.22), we may calculate the weak-shear-flow limit of, *inter alia*, the correlations within the set $\{\xi^4, \xi^5\}$,

$$\chi^{44}(\mathbf{k}) = J^{44}(\mathbf{k}), \tag{7.32}$$

$$\chi^{55}(\mathbf{k}) = J^{55}(\mathbf{k}), \tag{7.33}$$

$$\chi^{45}(\mathbf{k}) = -\frac{4\beta_2 D}{3BS_0(T)}\left[J^{44}(\mathbf{k}) + J^{45}(\mathbf{k}) + J^{55}(\mathbf{k})\right], \tag{7.34}$$

where $\chi^{54}(\mathbf{k}) = \chi^{45}(\mathbf{k})$, and where $J^{kl}(\mathbf{k})$ is given by Eq. (7.27), with masses

$$m^4 = \tfrac{1}{4}[B - 3CS_0(T)]\,rD, \tag{7.35}$$

$$m^5 = -\tfrac{3}{2}BS_0(T) - [B - 3CS_0(T)]\,rD. \tag{7.36}$$

Using polarized light scattering one can isolate the fluctuations of these modes. Perhaps the most striking effect of weak shear flow on the nematic state is the acquisition by the Goldstone mode $\chi^{44}(\mathbf{k})$, Eq. (7.35), of a mass proportional to the strain rate D. Also noteworthy is the fact that the correlation $\chi^{45}(\mathbf{k})$ $[= \chi^{54}(\mathbf{k})]$ is now nonzero and, as we see from Eqs. (7.27) and (7.34), is approximately a sum of three independent Ornstein-Zernicke forms $(m^i + m^j + 2L_1k^2)^{-1}$. In other words, modes that would be independent in equilibrium are coupled by the flow. The same calculation for the 3×3 sector, $\mathbf{M}^{(1A)}$, yields qualitatively identical behavior, with a shift in the mass of the Goldstone mode $\chi^{33}(\mathbf{k})$ proportional to D, and shear-induced off-diagonal correlations.

(ii) For $T \geq T_{I\text{-}N}(D)$ we see from Eq. (5.4b) that $S_1 \simeq S_2 \sim D$ so that the mass matrix becomes

$$\mathbf{M} = A(T)\,\mathbf{I} + \mathbf{M}^{(1)}\,D + O(D^2), \tag{7.37}$$

in which

$$\mathbf{M}^{(1)} = \begin{pmatrix} B\tilde{S}_1 & \frac{1}{\sqrt{3}}B\tilde{S}_1 & -\sqrt{3}\beta_2 & 0 & 0 \\ \frac{1}{\sqrt{3}}B\tilde{S}_1 & -B\tilde{S}_1 & \beta_2 & 0 & 0 \\ \sqrt{3}\beta_2 & -\beta_2 & 0 & 0 & 0 \\ 0 & 0 & 0 & B\tilde{S}_1 & -\beta_2 \\ 0 & 0 & 0 & \beta_2 & -B\tilde{S}_1 \end{pmatrix}, \tag{7.38}$$

where $\tilde{S}_1$ is given by

$$\tilde{S}_1 \equiv \lim_{D\to 0} S_1/D = \beta_1\beta_2/2A(T). \tag{7.39}$$

Just as for $T < T_{I\text{-}N}(D)$, in the present case shear flow gives the diagonal modes an additional mass contribution proportional to the strain rate, and induces off-diagonal correlations.

D. Light scattering near the nonequilibrium critical point

In our linear approximation, the eigenvalues of $\mathbf{M}$ govern the time dependence of the modes of $\delta Q_{\alpha\beta}$. For a stable steady state the real parts of the eigenvalues of $\mathbf{M}$ are non-negative, whereas for an unstable state $\mathbf{M}$ has one or more eigenvalues (i.e., masses) with a negative real part. In shear flow, the (massless) Goldstone modes of the equilibrium nematic acquire a mass, and all eigenvalues have a positive real part, except at the nonequilibrium critical point, where there is a single massless mode corresponding to the critical mode. This mode is a superposition of the modes $\{e^1_{\alpha\beta}, e^2_{\alpha\beta}, e^3_{\alpha\beta}\}$, and corresponds to simultaneously adjusting the *degree* of order (i.e., changing S_1 and S_2) and *rotating* the director $\hat{\mathbf{n}}$ in the shear plane, as can be seen from Eqs. (A3) and (A4). This massless mode can be understood physically in the following way. In the presence of shear flow the steady-state orientation of the director $\hat{\mathbf{n}}$ lies in the shear plane at a certain angle. Now consider a departure from this stationary alignment. A rotation of $\hat{\mathbf{n}}$ *within* the shear plane will be rapidly suppressed by the flow, which exerts a restoring torque. However, a tilt *out* of the shear plane will not be so strongly affected by flow, suggesting more frequent and larger-amplitude excursions out of the plane than within it. Hence, the molecular orientation distribution is biaxial.

The nonequilibrium transition occurs between a state governed primarily by the flow (a rather weakly ordered, biaxial state) and a state governed primarily by the thermodynamics of the *I-N* transition (a strongly ordered, more uniaxial state). These two states differ in their amplitudes S_1 and S_2, and in their in-plane alignment of $\hat{\mathbf{n}}$. As the critical point is approached these states merge, and the massless mode is thus the mode which interpolates between the confluent states, hence involving variations in the two amplitudes and the in-plane orientation of $\hat{\mathbf{n}}$. One may isolate the critical mode, experimentally, by selecting polarizations in the shear plane, for which, as we see from Eqs. (A3) and (C1), fluctuations involving the amplitudes ξ^4 and ξ^5 do not contribute; see Fig. 10.

Near the nonequilibrium critical point we may identify two distinct regimes, corresponding to wave numbers large or small compared with the wave number characteristic of the critical point, k_{D^*}.

1. *Small-strain-rate, large-wave-vector limit*

For $(k/k_D)^2 \gg |\hat{k}_x|$, i.e., $D \ll L_1 k^2/\beta_2|\hat{k}_x|$, it is legitimate to approximate $J^{kl}(\mathbf{k})$ by the leading (i.e., Ornstein-Zernicke) form, Eq. (7.27), so that $\boldsymbol{\chi}(\mathbf{k})$ is then a sum of such terms, Eq. (7.22). As the critical point is approached this superposition is dominated at long wavelengths by the zero mass term, i.e.,

$$\chi^{ij}(\mathbf{k}) \sim \Gamma^{ij,11}\,J^{11}(\mathbf{k}) \sim \frac{\Gamma^{ij,11}}{m^1 + L_1 k^2} \tag{7.40}$$

for the sector $(i,j = 1,2,3)$, where we have chosen m^1 to label the (vanishing) mass of the critical mode. Hence, in this wavelength regime we expect that, as the critical point is approached, the system behaves qualitatively like the LG system near its equilibrium critical point, except that the observation of divergent fluctuations becomes *polarization dependent*. For example, if we choose $\hat{\mathbf{p}}||\hat{\mathbf{m}}$ and $\hat{\mathbf{p}}'||\hat{\mathbf{z}}$, we find from Eq. (C3) that $d\sigma/d\Omega \sim \langle|\xi^5(\mathbf{k})|^2\rangle$, which does *not* diverge at the critical point. Note also from Eq. (7.27) that for $k \gg k_D$ the scattering is isotropic in $\mathbf{k}$ space. This coincides with the intuitive picture, proposed by OK [1], that shorter-wavelength fluctuations decay via thermodynamic relaxation before shear flow can act to suppress them. (Recall that within the one-constant approximation, equilibrium scattering properties are isotropic in $\mathbf{k}$ space.)

2. *Large-strain-rate, small-wave-vector limit*

In the limit $(k/k_D)^2 \ll |\hat{k}_x|$, or equivalently $D \gg L_1 k^2/\beta_2|\hat{k}_x|$, we may approximate $J^{kl}(\mathbf{k})$ by

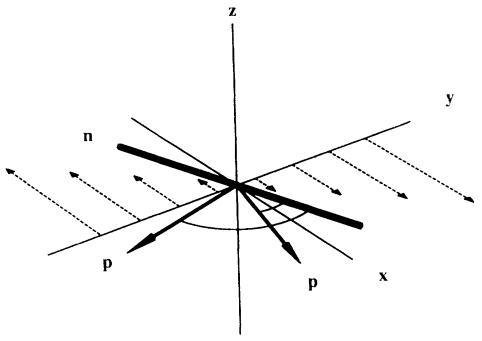

FIG. 10. Geometry for observing fluctuations in the critical mode via light scattering near the critical point. The polarization vectors $\hat{\mathbf{p}}$ and $\hat{\mathbf{p}}'$ lie in the shear plane, and the broken arrows denote the velocity field.

$$J^{kl}(\mathbf{k}) \simeq \frac{k_B T \Gamma(\frac{1}{3})}{L_1 k_D^2}\left(\frac{2k_D}{3k_x}\right)^{2/3}\left[1-\frac{\Gamma(\frac{2}{3})}{\Gamma(\frac{1}{3})}\left(\frac{3}{2}\right)^{1/3}\frac{(m^k+m^l+2L_1k^2)}{L_1(k_x k_D^2)^{2/3}}-\frac{(18)^{1/3}}{\Gamma(\frac{1}{3})}\frac{k_y}{(k_x k_D^2)^{1/3}}+\cdots\right]. \quad (7.41)$$

In this regime correlations are strongly suppressed by the flow, $J^{kl}(\mathbf{k}) \sim D^{-2/3}$, and are independent, in the large-strain-rate limit, of the incident and scattering polarizations (i.e., the indices l and k). Note also the strong anisotropy: fluctuations at small k_x are enhanced, reflecting their relative immunity to deformation by advection; see Fig. 11.

E. Discussion of fluctuations

To summarize, we find the following behavior from an analysis of linear fluctuations at the critical point: (i) polarization-dependent divergent fluctuations, (ii) anisotropic correlations at long wavelengths, and (iii) isotropic scattering at small wavelengths. Figure 12 shows a plot of $\chi^{11}(\mathbf{k})$ at the critical point, as calculated from Eqs. (7.22) and (7.23), exhibiting the anisotropy for small wave vectors which gives way to an isotropic profile for large wave vectors.

We have shown that the effects of shear flow on the I-N transition can be considerable, inducing a variant of critical opalescence near the nonequilibrium critical point. The spatial anisotropy of the correlations reflects the role of shear flow in selecting certain fluctuations for destruction, a general feature which is also important for the LG and I-L transitions. The polarization dependence of the anomalous scattering is a feature of the critical point not present at the LG critical point. This behavior follows directly from the additional role of shear flow, peculiar to the I-N system, as an *ordering* field which acts on particular degrees freedom within the five-dimensional order-parameter space. This ordering field imposes biaxial nematic order on both the high- and low-temperature phases (which differ in nematic order and strain rate) and, when sufficiently strong, induces a continuous transition. Our linear theory predicts that through a proper choice of polarization configurations one may selectively probe fluctuations which either exhibit divergences at or remain smooth through the critical point. A more refined treatment which accounts for nonlinear couplings between modes would lead to additional singular correlations.

It should be noted that one also expects polarization-dependent critical fluctuations near the equilibrium critical point induced in a fluid of nematogens (of positive magnetic susceptibility) by an applied magnetic field. However, the sensitivity to polarization is then determined neither by the amplitude of the magnetic field nor by the temperature. Therefore, the nature of the critical point in the equilibrium nematogenic fluid differs qualitatively from that in the nonequilibrium fluid of nematogens under shear flow. The critical mode of the equilibrium nematic system in a field is a pure *amplitude* mode of the nematic system order parameter, whereas that of the flowing nematic system is a linear combination of *amplitude* and *orientation* modes. (See Ref. [65] for measurements distinguishing amplitude from orientation modes near the equilibrium I-N transition.) A manifestation of this peculiarity occurs when one considers the discontinuity in the nematic order parameter across the coexistence line in the nonequilibrium phase diagram. We find that the orientation of the principal axes of the nematic order parameter spontaneously rotate as one moves away from the critical point, e.g., along the coexistence line. Thus, in order to parametrize correctly the approach to the critical point it is necessary to project the nematic order-parameter discontinuity on to the critical mode.

A second issue which superficially distinguishes the stressed fluid of nematogens from the stressed LG concerns the strain rate at which strong fluctuations occur. In the LG one may, in principle, observe strong fluctuations at any strain rate, by making a strain-rate-dependent tuning of the pressure and temperature so as to locate the system near to its critical point. Thus, one can in essence adjust k_D. Now suppose that the exper-

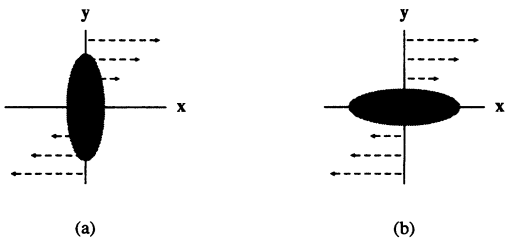

FIG. 11. Advection of fluctuations in shear flow: (a) is intended to represent a fluctuation with $|k_x| \gg |k_y|$, which is quickly suppressed by the flow; (b) represents a fluctuation with $|k_x| \ll |k_y|$, which is more robust under flow.

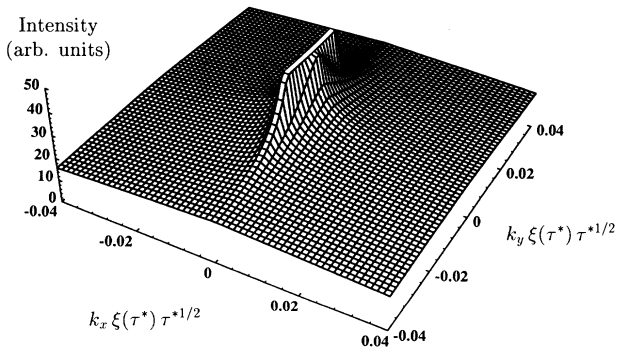

FIG. 12. Scattering intensity at the critical point for the mode χ^{11}, for material parameters $B = -1.2C$, and $\beta_1 = 0.9$. Wave vectors are plotted in dimensionless units, $\bar{k} \equiv k\xi^*\tau^{*1/2}$, where $\xi^{*2} = L/a(T^* - T^-)$ gives the equilibrium correlation length.

imental conditions determine the order of magnitude of the "momentum" transfer k during a scattering experiment, e.g., momentum transfers in the optical range. Then, by adjusting k_D one can probe all three regimes, with k_D larger, smaller, or comparable with k.

In contrast, for a given fluid of nematogens, and in the absence of a magnetic field, there is a specific material-dependent critical strain rate near which one can observe strong fluctuations. Hence, for experimental circumstances that dictate the order of magnitude of k we expect that near the critical point of certain materials one will find $k \gg k_D$, i.e., predominantly isotropic scattering, whereas for other materials the relevant limit will be $k \ll k_D$, so that light scattering would probe the anisotropy caused by the shear flow.

The distinction between LG and the fluid of nematogens, mentioned above, is only superficial. If one is prepared to impose an external magnetic field on the nematogens, in addition to shear stress, then one can observe strong fluctuations at any strain rate. The reason for this is that a magnetic field can induce a critical point even in the absence of shear stress [30]. Thus, there is a closed loop of critical points in the magnetic-field–shear-stress–temperature phase diagram. This loop interpolates between two extremes: (i) the equilibrium critical point (in the absence of stress but the presence of a strong magnetic field) for which the critical mode resides entirely within the amplitude sector of nematic order-parameter space; and (ii) the nonequilibrium critical point (in the absence of a magnetic field but the presence of strong stress), for which the critical mode includes both amplitude and orientational degrees of freedom. Hence, the combined application of shear stress and magnetic field may provide the most convenient experimental situation in which to bring to more readily accessible strain rates the flow-induced nonequilibrium critical point.

To illustrate the issue of wave-number regimes in zero magnetic field we present an alternative expression for the critical wave number. From Eq. (7.3) we see that the characteristic wave number at the critical point is given by

$$k_{D^*} = \sqrt{D^*\beta_2/L_1}\,. \tag{7.42}$$

As the dimensionless temperature τ and strain rate δ are given by $\delta = D\beta_2/C$ and $\tau = A(T)/C$, Eqs. (5.2a) and (5.2b), the characteristic wave number at the critical point is given by

$$k_{D^*}\,\xi^* = \sqrt{\delta^*/\tau^*}, \tag{7.43}$$

where $\xi^* = \sqrt{L_1/A(T^*)}$ is the *equilibrium* fluctuation correlation length associated with the nematic state at the *nonequilibrium* critical temperature τ^*. The critical parameters τ^* and δ^* are themselves functions of only two parameters: (i) the ratio B/C, which is a measure of the weakness of the first-order transition (because $\Delta S_1 = -2B/9C$ [30]), and (ii) the kinetic coefficient β_1, which is a ratio of rotational viscosities and is approximately material independent. Hence, we may roughly say that the characteristic wave number at the critical point depends on the weakness of the equilibrium first-order transition, and on the equilibrium correlation length at temperatures near the critical temperature.

Let us examine this length scale for low-molecular-weight systems such as MBBA. For the choice of parameters $B = -1.2\,C$ and $\beta_1 = 0.9$, representative of low-molecular-weight systems, we have found a ratio $\delta^*/\tau^* \sim 0.1$. Then the typical experimental value $\xi^* \sim 150$ Å [50], together with the shift $(T^*\!-\!T^-) \sim 1.0$ K (see Sec. V D), yields $k_D^* \sim 10^7$ m^{-1}. For comparison, light-scattering experiments typically explore wave numbers $k = 2k_0 \sin(\theta/2)$, where $k_0 \sim 10^7$ m^{-1} and θ is the scattering angle. Hence, we expect thermotropic materials to have critical wave numbers in the readily observable range so one may observe fluctuations at wave vectors both greater (yielding isotropic scattering) and smaller (yielding anisotropic critical scattering) wavelengths than the characteristic wavelength k_D^*.

VIII. CONCLUDING REMARKS

A. Summary of results

In this paper we have presented a description of the influence of shear flow on the I-N transition in fluids of thermotropic nematogens. In doing this, we have discussed the time evolution of the nematic order parameter and fluid velocity, identified homogeneous nonequilibrium steady states, examined inhomogeneous steady states, and constructed the first-order phase boundary in the nonequilibrium phase diagram, analyzed the nonequilibrium critical point, developed a theory of fluctuations about biaxial states, and examined polarized light scattering. As we have seen, coherent macroscopic shear flow can significantly influence the nature of the I-N transition, by inducing nematic alignment at the molecular level and also by distorting thermal fluctuations through advection.

From the deterministic coupled equations of motion we have established the following points. The stable homogeneous steady states exhibit several features characteristic of equilibrium first-order phase transitions, including a discontinuous transition between states, accompanied by a region of the phase diagram possessing two states, each locally stable with respect to homogeneous fluctuations, and a critical point at which the transition becomes continuous and singularities are found in the response to temperature and external probes. There exists an analog of a coexistence line in the applied-stress–temperature phase diagram, found by analyzing states inhomogeneous in one spatial dimension; within our approximations, the behavior near the critical point is classical.

From the linearized stochastic dynamics of nematic order-parameter fluctuations about locally stable nonequilibrium steady states, but neglecting fluctuations in the velocity field, we have found the following points. Flow destroys the massless Goldstone modes of the equilibrium uniaxial nematic state, as it should, due to its biaxial symmetry, and introduces anisotropy into the fluctuation correlations. Flow also *induces* a massless fluctuation mode at the nonequilibrium critical point, which

may be probed by specific choices of polarizations in elastic light-scattering experiments. The critical behavior is associated with a single mode, which, unlike conventional Ising-like critical modes, involves both amplitude and orientation variations.

B. Assumptions and approximations

We have made a number of significant assumptions, which we now review. In our analysis of homogeneous and inhomogeneous states, and the nonequilibrium phase diagram, we have entirely neglected the role of thermal fluctuations, except with regard to the issue of local stability. Even in this regard we have been incomplete, especially concerning the issue of fluctuations at constant applied stress and spatially inhomogeneous fluctuations. Thus, apart from the transition that we have explicitly been considering, we have assumed that the system exhibits smooth behavior, as the shear stress and temperature are varied. Nor have we entertained the quite reasonable possibility, at least for certain ranges of the material and control parameters, of transitions to states with qualitatively different flow patterns. Many such possibilities can be envisaged, including nonlinear dynamical instabilities to nonstationary states at high shear stress, e.g., giving rise to so-called "tumbling" states. Such transitions have been observed in certain low-molecular-weight systems, above a critical strain rate [66]. One should also consider the interesting possibility of a transition to a tumbling state, as the temperature is lowered. Recalling the alignment condition, Eq. (5.1c), $2\beta_1 \cos 2\theta = 3S_1 + S_2$, we observe that for sufficiently strong ordering in S_1 and S_2, this condition cannot be satisfied, and one does not expect to find a stationary state. Such behavior has been observed by Gähwiller in measurements of the temperature-dependence of the Leslie coefficients [49], and has recently been discussed by Larson, for the case of liquid-crystalline polymers [39].

We have also neglected to face the possibility of instabilities associated primarily with the shear flow itself, such as the Taylor-Couette instability [9], which occurs for simple fluids in Couette flow. It would be most interesting to investigate how such instabilities are affected by the stress induced on the fluid by nematic ordering. Related shear instabilities, such as those concerning undulations in sliding stratified fluids, have been discussed for smectic fluids in shear flow [67]. Such processes could certainly be of relevance to interfaces between coexisting homogeneous states; we have not as yet performed calculations rich enough to encounter such phenomena. In addition, as we have essentially been focusing on bulk properties, we have not attempted to investigate the role of boundary conditions either on the fluid velocity or, more importantly, on the nematic order parameter. Moreover, we have omitted any critical discussion of heat flow, assuming that the thermal diffusivity is sufficiently high that the temperature remains, for all practical purposes, uniform.

In our discussion of the fluctuations near the critical point we have made at least three crucial assumptions. First, we have introduced a noise source which obeys the fluctuation-dissipation theorem. Thus, we have assumed that the nonequilibrium microscopic fluctuations are governed by their equilibrium probability distribution. This issue is a fundamental one in nonequilibrium physics, and is presently an active and controversial subject of research [68]. Second, we have treated fluctuations at the linear level, thus omitting nonlinear couplings between fluctuating degrees of freedom. Thus, we are unable to probe the critical point at a level beyond the analog of the Gaussian approximation. Third, even within this Gaussian approximation, we have omitted fluctuations in the velocity and, less crucially, the density, concentrating solely on nematic fluctuations.

C. Future directions

In this final section we mention certain issues which we consider to be important and worthy of future investigation. (This list is certainly not intended to be exhaustive.) First, the issue of universality and scaling in the vicinity of the nonequilibrium critical point should be addressed using renormalization-group ideas, and the experimental consequences of non-Gaussian fluctuations for light-scattering and viscosity anomalies should be elucidated. Second, the impact of applied magnetic fields on the nonequilibrium phase transition should be ascertained. Third, the stability, structure, and excitations of interfaces between coexisting nonequilibrium states should be analyzed, and spatio-temporal instabilities of such interfaces should be considered. Fourth, the kinetics of the discontinuous nonequilibrium phase transition should be studied, including nonequilibrium metastability near coexistence, and nonequilibrium spinodal decomposition beyond stability limits. Fifth, the theoretical picture presented here should be enlarged to encompass concentration fluctuations, so that lyotropic systems may be addressed.

We have seen that the typical critical strain rate for thermotropic liquid crystals is of the order of 10^5 s^{-1}. Such strain rates are comparable with the currently accessible experimental limit. They are also high enough to make dynamical instabilities a serious issue: such instabilities could set in before the critical point is reached. Recalling the form for the dimensionless strain rate, $\delta = D\beta_2/C$, we see that a larger viscosity β_2 enables the critical point δ^* to be reached with smaller strain rates D. Ideal candidates, then, are mesogenic materials possessing high viscosities: lyotropic systems, such as solutions of the tobacco mosaic virus [i.e., TMV, rigid rodlike objects of length $\sim$ 1800 Å), have much higher viscosities than smaller (length $\sim$ 20 Å) low-molecular-weight thermotropic materials, and are known to be very sensitive to flow gradients [40].

In extending our dynamical treatment to lyotropic systems, the composition should be treated as an additional, kinematically independent hydrodynamic variable. Additionally, the equilibrium I-N transition in lyotropic systems can typically be controlled by both temperature and concentration, and the specific volume discontinuity at the transition is not negligible, unlike thermotropic systems. Hence, there are regions in the temperature-

concentration phase diagram in which phase-coexistence occurs, because of the large concentration difference between isotropic and nematic phases, thus adding a level of complexity to the problem. Finally, the order-parameter discontinuity is usually larger in lyotropic systems ($\Delta S_1 \sim 0.5$ for TMV, compared to $\Delta S_1 \sim 0.3$ for MBBA) [40], which makes the Landau–de Gennes expansion less reliable. Nevertheless, the prospect of flow-induced effects at comparatively low strain rates makes lyotropic systems attractive.

To conclude, we have attempted to present a coherent treatment of the isotropic-nematic transition in thermotropic fluids of nematogens under applied shear stress, which illustrates the similarities and differences between equilibrium and nonequilibrium phase transitions and critical phenomena. The tensorial nature of nematic ordering brings with it a wealth of interesting physical phenomena, and makes nematic systems a natural environment in which to study the effects of flow on phase transitions. It also brings a considerable technical complexity to the subject which guarantees that much remains to be revealed by future investigators.

ACKNOWLEDGMENTS

It is a pleasure to thank Martin Grant, Nigel Goldenfeld, Fong Liu, and particularly Yoshi Oono for several helpful conversations, and Stephen Wolfram for providing us with a copy of MATHEMATICA™. In addition, we thank the staff of the Center for Computation at the University of Illinois Materials Research Laboratory (UIUC MRL) for their patient advice, where much of the numerical work reported here was undertaken. This project was supported in part by the U.S. National Science Foundation through Grants No. NSF-DMR-89-20538 (administered through UIUC MRL), and No. NSF-DMR-91-22385, and No. NSF-DMR-91-57018.

APPENDIX A: ORDER-PARAMETER DECOMPOSITION

In this appendix we define the parametrization of the order parameter used throughout this paper. First, we consider the order parameter for a general biaxial state,

$$Q_{\alpha\beta} = \tfrac{3}{2} S_1 (n_\alpha n_\beta - \tfrac{1}{3}\delta_{\alpha\beta}) + \tfrac{1}{2} S_2 (m_\alpha m_\beta - l_\alpha l_\beta), \qquad \text{(A1)}$$

where $\hat{\mathbf{n}}$ is the director, $\hat{\mathbf{m}}$ is the subdirector which identifies the asymmetry in the distribution of rod orientations relative to $\hat{\mathbf{n}}$, and $\{\hat{\mathbf{n}}, \hat{\mathbf{m}}, \hat{\boldsymbol{l}}\}$ form a right-handed orthonormal triad [29]. The amplitudes S_1 and S_2 parametrize the strength of uniaxial and biaxial ordering, respectively. Upon performing a variation in $Q_{\alpha\beta}$, it is possible to expand a deviation $\delta Q_{\alpha\beta}$ in a convenient basis of orthonormal traceless symmetric tensors $\{e^i_{\alpha\beta}\}_{i=1}^5$, with amplitudes $\{\xi^i\}_{i=1}^5$ [57]:

$$\delta Q_{\alpha\beta} = \sum_{i=1}^{5} \xi^i \, e^i_{\alpha\beta}, \qquad \text{(A2)}$$

where

$$\begin{aligned}
e^1_{\alpha\beta} &= \sqrt{3/2}\,(n_\alpha n_\beta - \tfrac{1}{3}\delta_{\alpha\beta}),\\
e^2_{\alpha\beta} &= \sqrt{1/2}\,(m_\alpha m_\beta - l_\alpha l_\beta),\\
e^3_{\alpha\beta} &= \sqrt{1/2}\,(n_\alpha m_\beta + m_\alpha n_\beta),\\
e^4_{\alpha\beta} &= \sqrt{1/2}\,(n_\alpha l_\beta + l_\alpha n_\beta),\\
e^5_{\alpha\beta} &= \sqrt{1/2}\,(m_\alpha l_\beta + l_\alpha m_\beta),
\end{aligned} \qquad \text{(A3)}$$

and orthonormality is defined by $e^i_{\alpha\beta}\, e^j_{\beta\alpha} = \delta^{ij}$. In obtaining this expansion we have only allowed variations which maintain the orthonormality of the directors. The amplitudes $\{\xi^i\}$ are related to the explicit variations in the order parameter through

$$\begin{aligned}
\xi^1 &= \sqrt{3/2}\;\delta S_1,\\
\xi^2 &= \delta S_2/\sqrt{2},\\
\xi^3 &= (3S_1 - S_2)\,\hat{\mathbf{m}}\cdot\delta\hat{\mathbf{n}}\,/\sqrt{2},\\
\xi^4 &= (3S_1 + S_2)\,\hat{\mathbf{l}}\cdot\delta\hat{\mathbf{n}}\,/\sqrt{2},\\
\xi^5 &= \sqrt{2}\;S_2\,\hat{\mathbf{l}}\cdot\delta\hat{\mathbf{m}}.
\end{aligned} \qquad \text{(A4)}$$

Note that ξ^1 and ξ^2 parametrize *amplitude* fluctuations, whereas ξ^3, ξ^4, and ξ^5 parametrize *orientation fluctuations*. For fluctuations along $e^1_{\alpha\beta}$ the degree of order along the director increases; such fluctuations correspond to the standard amplitude fluctuations found in uniaxial nematics. Fluctuations along $e^2_{\alpha\beta}$ produce a change in the asymmetry of the distribution about $\hat{\mathbf{n}}$, i.e., a change in the biaxiality of the state. Fluctuations along $e^3_{\alpha\beta}$ and $e^4_{\alpha\beta}$ correspond to the two directions in which to rotate $\hat{\mathbf{n}}$, and $e^5_{\alpha\beta}$ fluctuations correspond to a rotation of the subdirector $\hat{\mathbf{m}}$ about $\hat{\mathbf{n}}$. For $S_2 = 0$ the fluctuations $e^3_{\alpha\beta}$ and $e^4_{\alpha\beta}$ represent the Goldstone modes found in uniaxial nematic states.

APPENDIX B: INTEGRATION OF STATIONARITY CONDITION

Consider the following system of ordinary differential equations:

$$\frac{d}{dq}\mathbf{Z}(q) = \mathbf{K}(q)\,\mathbf{Z}(q) + \mathbf{Z}(q)\,\mathbf{K}^{\mathrm{T}}(q) + \mathbf{G}(q)\,, \qquad \text{(B1)}$$

in which $\mathbf{Z}$, $\mathbf{K}$, and $\mathbf{G}$ are $N \times N$ matrix functions of q, with $\mathbf{K}$ and $\mathbf{G}$ supposed known, and $\mathbf{Z}$ sought. To find the solution $\mathbf{Z}(q)$, subject to the boundary condition $\mathbf{Z}(q_0) = \mathbf{Z}_0$, write the solution in the form

$$\mathbf{Z}(q) = \mathbf{Q}(q)\,\mathbf{Z}_0\,\mathbf{Q}^{\mathrm{T}}(q) + \mathbf{Q}(q)\,\mathbf{W}(q)\,\mathbf{Q}^{\mathrm{T}}(q), \qquad \text{(B2)}$$

with $\mathbf{Q}(q)$ satisfying

$$\frac{d}{dq}\mathbf{Q}(q) = \mathbf{K}(q)\,\mathbf{Q}(q), \qquad \text{(B3)}$$

subject to the initial condition $\mathbf{Q}(q_0) = \mathbf{I}$, in which $\mathbf{I}$ is the $(N \times N)$ identity matrix. Then $\mathbf{W}(q)$ satisfies

$$\frac{d}{dq}\mathbf{W}(q) = \mathbf{Q}^{-1}(q)\,\mathbf{G}(q)\,\left(\mathbf{Q}^{\mathrm{T}}\right)^{-1}(q)\,, \qquad \text{(B4)}$$

subject to the initial condition $\mathbf{W}(q_0) = \mathbf{O}$. Equation (B4) is readily integrated, giving the solution

$$\begin{aligned}
\mathbf{Z}(q) = {}& \mathbf{Q}(q)\,\mathbf{Z}_0\,\mathbf{Q}^{\mathrm{T}}(q)\\
&+ \int_{q_0}^{q} dk\,\mathbf{Q}(q)\,\mathbf{Q}^{-1}(k)\,\mathbf{G}(k)\,\left(\mathbf{Q}^{\mathrm{T}}\right)^{-1}(k)\,\mathbf{Q}^{\mathrm{T}}(q)\,,
\end{aligned} \qquad \text{(B5)}$$

in terms of (the as yet unknown) matrix $\mathbf{Q}(k)$. Equation (B3) is also readily integrated, at least formally, giving

$$\mathbf{Q}(q) = \hat{T} \exp\left\{ \int_{q_0}^{q} dk\, \mathbf{K}(k) \right\}, \tag{B6}$$

where $\hat{T}$ denotes the "time-ordering" operation. If it should happen that $\mathbf{K}(k)$ commutes with itself throughout the interval $q_0 \le k \le q$ then the time-ordering operation is redundant, and we have the explicit solution

$$\mathbf{Q}(q) = \exp\left\{ \int_{q_0}^{q} dk\, \mathbf{K}(k) \right\}. \tag{B7}$$

In this case, the complete solution, Eq. (B5), reduces to

$$\begin{aligned}\mathbf{Z}(q) = {} & \exp\left\{ \int_{q_0}^{q} dk\, \mathbf{K}(k) \right\} \mathbf{Z}_0 \exp\left\{ \int_{q_0}^{q} dk\, \mathbf{K}^{\mathrm{T}}(k) \right\} \\ & + \int_{q_0}^{q} dp \exp\left\{ \int_{p}^{q} dk\, \mathbf{K}(k) \right\} \\ & \times \mathbf{G}(p) \exp\left\{ \int_{p}^{q} dk\, \mathbf{K}^{\mathrm{T}}(k) \right\}. \end{aligned} \tag{B8}$$

For the application of this solution to fluctuation correlations in flowing nematogens we identify $\mathbf{Z}(q)$ with $\boldsymbol{\chi}(\mathbf{k})|_{k_y=q}$ in Eq. (7.19). We then apply the boundary condition that $\mathbf{Z}_0 = \mathbf{Z}(q_0) = \mathbf{O}$ at $q_0 = \infty$, because the gradient free energy suppresses spatial variations in the nematic order parameter at extremely short length scales. Finally, two straightforward changes of integration variables [from p to t with $-t/2\beta_2 = (k_y - p)/Dk_x$ and from k to s with $-s/2\beta_2 = (k_y - k)/Dk_x$] yield the solution Eq. (7.20).

APPENDIX C: POLARIZATION CONFIGURATIONS

In this appendix we present specific expressions for the differential cross section for elastic light scattering for four polarization configurations of interest. In the following, expressions $\hat{\mathbf{p}}$ and $\hat{\mathbf{p}}'$ are, respectively, the polarizations of the incoming and outgoing light; $\mathbf{k}$ is the difference between the incident and scattered wave vectors; the shear plane contains $\hat{\mathbf{n}}$ and $\hat{\mathbf{m}}$; and $\hat{\boldsymbol{l}} = \hat{\mathbf{n}} \times \hat{\mathbf{m}}$. These expressions are constructed from Eq. (7.8).

(i) Polarizations in the shear plane ($\hat{\mathbf{p}} \perp \hat{\boldsymbol{l}}$, $\hat{\mathbf{p}}' \perp \hat{\mathbf{z}}$; $\hat{\mathbf{p}} \cdot \hat{\mathbf{n}} = \cos\theta$, $\hat{\mathbf{p}}' \cdot \hat{\mathbf{n}} = \cos\theta'$); see Fig. 10:

$$\begin{aligned}\frac{d\sigma}{d\Omega} \sim {} & \tfrac{1}{6} \langle |\xi^1(\mathbf{k})|^2 \rangle (2\cos\theta\cos\theta' - \sin\theta\sin\theta')^2 + \tfrac{1}{2} \langle |\xi^2(\mathbf{k})|^2 \rangle \sin^2\theta \sin^2\theta' + \tfrac{1}{2} \langle |\xi^3(\mathbf{k})|^2 \rangle \sin^2(\theta + \theta') \\ & + \langle \xi^2(\mathbf{k})\, \xi^3(-\mathbf{k}) \rangle \sin(\theta + \theta') \sin\theta \sin\theta' + \frac{1}{\sqrt{3}} \langle \xi^1(\mathbf{k})\, \xi^3(-\mathbf{k}) \rangle \sin(\theta + \theta')(2\cos\theta\cos\theta' - \sin\theta\sin\theta') \\ & + \frac{1}{\sqrt{3}} \langle \xi^1(\mathbf{k})\, \xi^2(-\mathbf{k}) \rangle \sin\theta \sin\theta' (2\cos\theta\cos\theta' - \sin\theta\sin\theta'). \end{aligned} \tag{C1}$$

(ii) Polarizations in the $\boldsymbol{l}$-$\mathbf{n}$ plane ($\hat{\mathbf{p}} \perp \hat{\mathbf{m}}$, $\hat{\mathbf{p}}' \perp \hat{\mathbf{m}}$; $\hat{\mathbf{p}} \cdot \hat{\mathbf{n}} = \cos\phi$, $\hat{\mathbf{p}}' \cdot \hat{\mathbf{n}} = \cos\phi'$):

$$\begin{aligned}\frac{d\sigma}{d\Omega} \sim {} & \tfrac{1}{6} \langle |\xi^1(\mathbf{k})|^2 \rangle (2\cos\phi\cos\phi' - \sin\phi\sin\phi')^2 + \tfrac{1}{2} \langle |\xi^2(\mathbf{k})|^2 \rangle \sin^2\phi \sin^2\phi' + \tfrac{1}{2} \langle |\xi^4(\mathbf{k})|^2 \rangle \sin^2(\phi + \phi') \\ & - \langle \xi^2(\mathbf{k})\, \xi^4(-\mathbf{k}) \rangle \sin(\phi + \phi') \sin\phi \sin\phi' + \frac{1}{\sqrt{3}} \langle \xi^1(\mathbf{k})\, \xi^4(-\mathbf{k}) \rangle \sin(\phi + \phi')(2\cos\phi\cos\phi' - \sin\phi\sin\phi') \\ & - \frac{1}{\sqrt{3}} \langle \xi^1(\mathbf{k})\, \xi^2(-\mathbf{k}) \rangle \sin\phi \sin\phi' (2\cos\phi\cos\phi' - \sin\phi\sin\phi'). \end{aligned} \tag{C2}$$

(iii) Polarizations normal to the director ($\hat{\mathbf{p}} \perp \hat{\mathbf{n}}$, $\hat{\mathbf{p}}' \perp \hat{\mathbf{n}}$; $\hat{\mathbf{p}} \cdot \hat{\mathbf{m}} = \cos\varphi$, $\hat{\mathbf{p}}' \cdot \hat{\mathbf{m}} = \cos\varphi'$):

$$\begin{aligned}\frac{d\sigma}{d\Omega} \sim {} & \tfrac{1}{6} \langle |\xi^1(\mathbf{k})|^2 \rangle \cos^2(\varphi - \varphi') + \tfrac{1}{2} \langle |\xi^2(\mathbf{k})|^2 \rangle \cos^2(\varphi + \varphi') + \tfrac{1}{2} \langle |\xi^5(\mathbf{k})|^2 \rangle \sin^2(\varphi + \varphi') \\ & - \frac{1}{\sqrt{3}} \langle \xi^1(\mathbf{k})\, \xi^2(-\mathbf{k}) \rangle \cos(\varphi - \varphi') \cos(\varphi + \varphi') - \frac{1}{\sqrt{3}} \langle \xi^1(\mathbf{k})\, \xi^5(-\mathbf{k}) \rangle \sin(\varphi + \varphi') \cos(\varphi - \varphi') \\ & + \langle \xi^2(\mathbf{k})\, \xi^5(-\mathbf{k}) \rangle \sin(\varphi + \varphi') \cos(\varphi + \varphi'). \end{aligned} \tag{C3}$$

(iv) Polarizations normal to and parallel to $\hat{\mathbf{n}}$ ($\hat{\mathbf{p}} = \hat{\mathbf{n}}$, $\hat{\mathbf{p}}' \perp \hat{\mathbf{n}}$; $\hat{\mathbf{p}}' \cdot \hat{\mathbf{m}} = \cos\psi$):

$$\frac{d\sigma}{d\Omega} \sim \tfrac{1}{2} \langle |\xi^3(\mathbf{k})|^2 \rangle \cos^2\psi + \tfrac{1}{2} \langle |\xi^4(\mathbf{k})|^2 \rangle \sin^2\psi + \tfrac{1}{2} \langle \xi^3(\mathbf{k})\, \xi^4(-\mathbf{k}) \rangle \sin 2\psi. \tag{C4}$$

* Electronic-mail address: pdolmst@erenj.bitnet
† Electronic-mail address: p-goldbart@uiuc.edu
Also at Beckman Institute for Advanced Science and Technology, 405 North Mathews Avenue, Urbana, IL 61801.

[1] A. Onuki and K. Kawasaki, Ann. Phys. (N.Y.) **121**, 456 (1979).
[2] S. Hess, Z. Naturforsch. **31a**, 1507 (1976).

[3] P. D. Olmsted and P. Goldbart, Phys. Rev. A **41**, 4578 (1990).
[4] R. F. Bruinsma and C. R. Safinya, Phys. Rev. A **43**, 5377 (1991).
[5] M. E. Cates and S. T. Milner, Phys. Rev. Lett. **62**, 1856 (1989); C. M. Marques and M. E. Cates, J. Phys. (Paris) **51**, 1733 (1990).
[6] D. Beysens, M. Gbadamassi, and B. Moncef-Bouanz, Phys. Rev. A **28**, 2491 (1983); D. Beysens, R. Gastaud, and F. Decruppe, *ibid.* **30**, 1145 (1984).
[7] H. See, M. Doi, and R. Larson, J. Chem. Phys. **92**, 792 (1990).
[8] P. D. Olmsted and P. Goldbart, Mol. Cryst. Liq. Cryst. **198**, 265 (1991).
[9] S. Chandrasekhar, *Hydrodynamic and Hydromagnetic Stability* (Clarendon, Oxford, 1961).
[10] S.-K. Ma, *Modern Theory of Critical Phenomena* (Benjamin, Reading, MA, 1971).
[11] L. D. Landau and E. M. Lifshitz, *Statistical Physics Part 1* (Pergamon, Oxford, 1980).
[12] P. D. Olmsted and P. Goldbart, in Proceedings of 1991 Fall Meeting of the Materials Research Society (Symposium O), Boston, 1991, edited by E. Sirota (Materials Research Society, Pittsburgh, in press).
[13] S.-Q. Wang and W. Gelbart, J. Chem. Phys. **90**, 597 (1989).
[14] K. G. Wilson and J. B. Kogut, Phys. Rep. **12C**, 75 (1974).
[15] B. Schmittmann, Int. J. Mod. Phys. B **4**, 2269 (1991); S. Katz, J. L. Lebowitz, and H. Spohn, Phys. Rev. B **28**, 1655 (1983); J. Stat. Phys. **34**, 497 (1984).
[16] J. Krug, J. L. Lebowitz, H. Spohn, and M. Q. Zhang, J. Stat. Phys. **44**, 535 (1986).
[17] H. K. Janssen and B. Schmittmann, Z. Phys. B **64**, 503 (1986); K.-T. Leung and J. L. Cardy, J. Stat. Phys. **44**, 567 (1986); **45**, 1087(E) (1986); H. van Beijeren and L. S. Schulman, Phys. Rev. Lett. **53**, 806 (1984).
[18] L. Leibler, Macromol. **13**, 1602 (1980).
[19] G. H. Fredricksen and E. Helfand, J. Chem. Phys. **87**, 697 (1987).
[20] S. A. Brazovskiĭ, Zh. Eksp. Teor. Fiz. **68**, 175 (1975) [Sov. Phys. JETP **41**, 85 (1975)].
[21] C. R. Safinya, E. B. Sirota, and R. J. Plano, Phys. Rev. Lett. **66**, 1986 (1991).
[22] F. M. Leslie, Quart. J. Appl. Math. **19**, 357 (1966); Arch. Ration. Mech. Anal. **28**, 265 (1968); J. L. Ericksen, Arch. Ration. Mech. Anal. **4**, 231 (1960); Phys. Fluids **9**, 1201 (1966).
[23] D. Forster, Phys. Rev. Lett. **32**, 1161 (1974).
[24] W. L. McMillan, Phys. Rev. A **9**, 1720 (1974).
[25] D. Thirumalai, J. Chem. Phys. **84**, 5869 (1986).
[26] S.-D. Lee, J. Chem. Phys. **86**, 6567 (1987).
[27] P. G. de Gennes, *The Physics of Liquid Crystals* (Clarendon, Oxford, 1975).
[28] D. Forster, *Hydrodynamic Fluctuations, Broken Symmetry, and Correlation Functions* (Benjamin, Reading, MA, 1975).
[29] T. C. Lubensky, Phys. Rev. A **2**, 2497 (1970).
[30] E. F. Gramsbergen, L. Longa, and W. H. de Jeu, Phys. Rep. **135C**, 195 (1986).
[31] P. G. de Gennes, Mol. Cryst. Liq. Cryst. **12**, 193 (1971).
[32] F. C. Frank, Discuss. Faraday Soc. **25**, 19 (1958).
[33] The "one-constant approximation" was originally applied to the Frank free energy for director distortions in a state with homogeneous magnitude of uniaxial nematic order [32]. The Frank free energy contains three elastic moduli (K_1, K_2, K_3), and within the one-constant approximation $K_1 = K_2 = K_3 = K$, which is equivalent to our approximation $L_2 = 0$.
[34] P. Goldbart and Ping Ao, Phys. Rev. Lett. **64**, 910 (1990).
[35] S. de Groot and P. Mazur, *Non-Equilibrium Thermodynamics* (Dover, New York, 1962).
[36] H. J. Kreuzer, *Nonequilibrium Thermodynamics and its Statistical Foundations* (Clarendon, Oxford, 1981).
[37] P. D. Olmsted, Ph.D. thesis, University of Illinois at Urbana-Champaign 1991.
[38] M. Doi and S. F. Edwards, *The Theory of Polymer Dynamics* (Oxford University Press, New York, 1989).
[39] R. G. Larson, Macromol. **23**, 3983 (1990).
[40] R. Oldenbourg, X. Wen, R. B. Meyer, and D. L. D. Caspar, Phys. Rev. Lett. **61**, 1851 (1988); S. Fraden, G. Maret, D. L. D. Caspar, and R. B. Meyer, *ibid.* **63**, 2068 (1989).
[41] See, *e.g.*, the Introduction, by A. S. Wightman, [in R. B. Israel *Convexity in the Theory of Lattice Gases*] (Princeton University Press, Princeton, NJ, 1978).
[42] H. Kramers, J. Chem. Phys. **14**, 415 (1946).
[43] It has been conjectured that nonequilibrium steady states obey a similar variational principle, namely, that of minimum entropy *production* [44]. This condition is obeyed by, e.g., steady-state heat flow in a system with open boundaries (to permit heat flow) and an applied temperature gradient [35,36]. However, the principle of minimum entropy production only asserts that the state of the system is a *local* minimum, in state space, of the entropy production [35,36]. It is not a criterion which determines global selection between locally stable states, in contrast with the equilibrium Maxwell construction (or minimization of the free energy).
[44] P. Glansdorff and I. Prigogine, *Thermodynamic Theory of Structure, Stability, and Fluctuations* (Wiley, London, 1971).
[45] See, e.g., L. D. Landau and E. M. Lifshitz, *Fluid Mechanics* (Pergamon, Oxford, 1979), particularly §15.
[46] This technique is similar to that used by Krug *et al.* [16] to find the coexistence line for the driven diffusive lattice gas.
[47] In addition to our detailed investigation of the fixed-boundary method, we have performed exploratory calculations using random initial conditions (in the absence of noise), and have found behavior consistent with the results of the fixed boundary method. In other words, we have observed behavior consistent with the existence of a unique coexistence temperature $T_{I\text{-}N}(\sigma_{xy})$, as described above. However, we have not investigated the role of random initial conditions in detail.
[48] W. H. Press, B. P. Flannery, S. A. Teukolsky, and W. T. Vetterling, *Numerical Recipes* (Cambridge University Press, Cambridge, England, 1986).
[49] C. Gähwiller, Mol. Cryst. Liq. Cryst. **20**, 301 (1973).
[50] T. W. Stinson and J. D. Litster, Phys. Rev. Lett. **30**, 688 (1973).
[51] While we occasionally give numerical results with high precision, such results are, of course, only as accurate as our initial (and perhaps crude) estimates of material

parameters.

[52] See, e.g., D. J. Wallace, in *Recent Advances in Field Theory and Statistical Mechanics*, edited by J.-B. Zuber and R. Stora (North-Holland, Amsterdam, 1984).

[53] T. W. Stinson and J. D. Litster, Phys. Rev. Lett. **25**, 503 (1970).

[54] D. L. Goodstein, *States of Matter* (Dover, New York, 1985).

[55] A. R. Khokhlov and A. N. Semenov, Macromol. **15**, 1272 (1982).

[56] Orsay Liquid Crystal Group, J. Chem. Phys. **51**, 816 (1969).

[57] A. Z. Patashinskiĭ and V. L. Pokrovskiĭ, Zh. Eksp. Teor. Fiz. **64**, 1445 (1973) [Sov. Phys. JETP **37**, 733 (1973)]; V. L. Pokrovskiĭ and E. I. Kats, *ibid.* **73**, 774 (1977) [**46**, 405 (1977)]; E. M. Aver'yanov, *ibid.* **97**, 855 (1990) [**70**, 479 (1990)].

[58] For a biaxial state, two independent traceless symmetric tensors can be built from $Q_{\alpha\beta}$ and $Q_{\alpha\beta}Q_{\beta\gamma}$. In general, each may contribute to $\epsilon_{\alpha\beta}$ with independent invariant normalizations. We assume that the stated contribution dominates, and note that this assumption is, in principle, experimentally testable.

[59] L. D. Landau and E. M. Lifshitz, *Electrodynamics of Continuous Media* (Pergamon, New York, 1960).

[60] N. G. van Kampen, *Stochastic Processes in Physics and Chemistry* (North-Holland, Amsterdam, 1981).

[61] P. N. Segrè, R. W. Gammon, J. V. Sengers, and B. M. Law, Phys. Rev. A **45**, 714 (1992); B. M. Law and J. V. Sengers, *ibid.* **41**, 816 (1990); B. M. Law, P. N. Segrè, R. W. Gammon, and J. V. Sengers, J. Stat. Phys. **57**, 531 (1989).

[62] P. D. Olmsted and P. M. Goldbart (unpublished).

[63] C. W. Gardiner, *Handbook of Stochastic Methods for Physics, Chemistry and the Natural Sciences* (Springer, Berlin, 1978).

[64] As **M** is a real and nonsymmetric matrix [see Eqs. (7.12–7.13)] parameters may conspire to render it nondiagonalizable. In such cases a different analysis must be employed; **M** is then singular and represents a projection onto a manifold of the five-dimensional fluctuation space. Such singularities occur at rare coincidences of the parameters, which we do not consider here. See, e.g., Harry Hochstadt, *Differential Equations: A Modern Approach* (Dover, New York, 1975).

[65] J. P. McClymer and P. H. Keyes, Phys. Rev. A **42**, 4764 (1990).

[66] P. E. Cladis and S. Torza, Phys. Rev. Lett. **35**, 1283 (1975); P. Pieranski and E. Guyon, Phys. Rev. A **9**, 404 (1974).

[67] J. Prost, Y. Pomeau, E. Guyon, J. Phys. (Paris) II **1**, 289 (1991).

[68] R. Graham, in *Order and Fluctuations in Equilibrium and Nonequilibrium Statistical Mechanics*, edited by G. Nicolis, G. Dewel, and J. W. Turner (Wiley, New York, 1981); R. Graham, in *Proceedings of Stochastic Processes in Non-Equilibrium Systems, Sitges, 1978*, Lecture Notes in Physics Vol. 84 (Springer-Verlag, Berlin, 1978).

[69] We remark that the critical temperature determined at fixed strain rate T_D^* is not in general equal to that determined at fixed stress T_σ^*. This discrepancy occurs because, although the same stationary states are available to the system, the stability of these states depends on whether it is the stress or the strain rate which is held constant during infinitesimal departures from a given state. The manifold of steady states can be thought of as forming part of a folded two-dimensional surface, embedded in a space spanned by temperature, nematic order parameter (which we temporarily envisage as one-dimensional), strain, rate, and stress. We interpret the critical point as the cusp which results when this folded surface is projected onto a coordinate surface spanned by the pair of control parameters temperature and stress. Alternatively, one might wish to identify the critical point as the cusp that results from a projection on to a surface spanned by an alternative pair of control parameters, e.g., temperature and strain rate. However, for any state the stress and strain rate are not independent. Therefore, as a consequence of exchanging stress for strain rate, we deform the coordinate surface onto which we project the fold, and therefore, in general, alter the state which when projected lies at the cusp. In particular, for different choices of control parameters the cusp will generally lie at different temperatures. Note, however, that the critical point is uniquely defined in terms of the end point of the coexistence line, which is determined only at a specified stress.

[70] G. Vertogen and W. H. de Jeu, *Thermotropic Liquid Crystals, Fundamentals* (Springer-Verlag, Berlin, 1988).

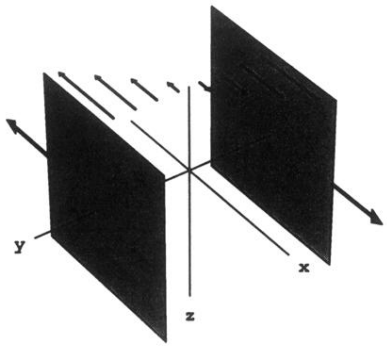

FIG. 1. Coordinate system for planar Couette flow, showing the boundary plates and fluid velocity field for a homogeneous state.

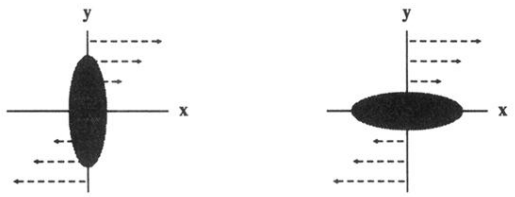

(a) (b)

FIG. 11. Advection of fluctuations in shear flow: (a) is intended to represent a fluctuation with $|k_x| \gg |k_y|$, which is quickly suppressed by the flow; (b) represents a fluctuation with $|k_x| \ll |k_y|$, which is more robust under flow.

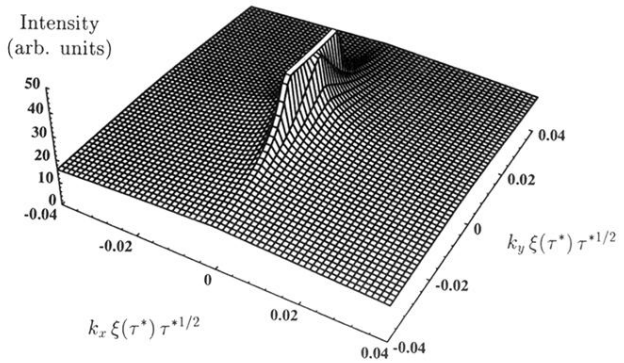

FIG. 12. Scattering intensity at the critical point for the mode χ^{11}, for material parameters $B = -1.2C$, and $\beta_1 = 0.9$. Wave vectors are plotted in dimensionless units, $\bar{k} \equiv k\,\xi^*\,\tau^{*1/2}$, where $\xi^{*\,2} = L/a(T^* - T^-)$ gives the equilibrium correlation length.

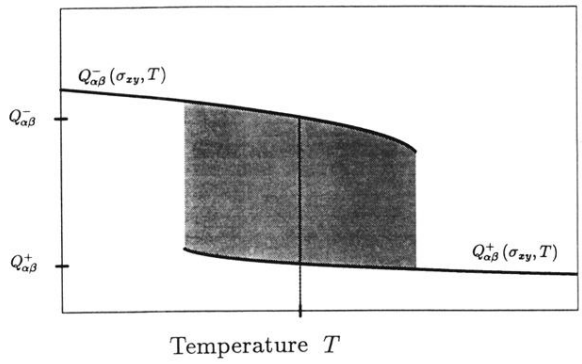

FIG. 4. Order parameter vs temperature for fixed applied stress. The branches labeled $Q^+_{\alpha\beta}(\sigma_{xy},T)$ and $Q^-_{\alpha\beta}(\sigma_{xy},T)$ are locally stable states. The shaded region is the two-state region, and the dotted line identifies the coexistence temperature as computed using the interface method described in Sec. VI). Due to the resolution of the plot, the turning points at the limits of stability do not appear.

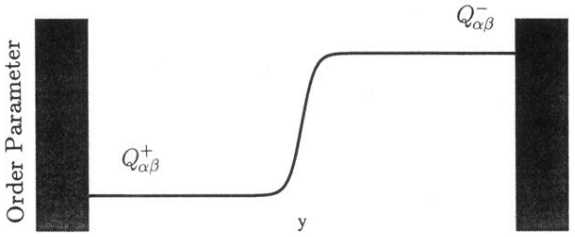

FIG. 5. Caricature of the order parameter vs spatial position y showing a stable interface at coexistence (four order-parameter dimensions have been suppressed). $Q^+_{\alpha\beta}$ refers to the order of the high-temperature state and $Q^-_{\alpha\beta}$ refers to the order of the low-temperature state.

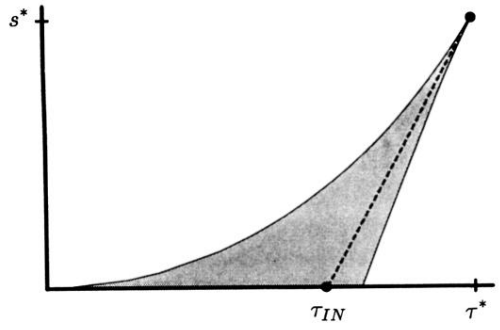

FIG. 9. Complete phase diagram in the reduced stress (s) vs reduced temperature (τ) phase diagram for material parameters $B = -1.2\,C$, $\beta_1 = 0.9$, $\beta_3 = 0.1\beta_2$, and $L_1/C = L_2/C = 10^4$ Å^2. The dashed line represents the coexistence line; the shaded region is the two-state region with two locally stable states; the solid lines mark the limits of stability for the high- and low-temperature states. The nonequilibrium critical point is located at $(\tau^*, s^*) \simeq (0.0817, 0.003\,795)$.